On the use of stochastic spectral methods in deep excavation inverse problems

Antonio Cañavate-Grimal*†, Antonio Falcó*, Pedro Calderón‡, Ignacio Payá-Zaforteza‡

11th May 2015

Abstract

The back analysis or inverse analysis of the field instrumentation data is a common technique to ascertain the design parameter validity in deep excavation projects. That analysis is a process full of uncertainties and relies greatly on the expert judgement. Furthermore, deep excavation geotechnical models tend to be computationally very expensive making the inverse analysis a very lengthy process. In this paper, a Bayesian-type methodology to solve inverse problems which relies on the reduction of the numerical cost of the forward simulation through stochastic spectral surrogate models is presented. The proposed methodology is validated with three calibration examples.

1 Introduction

Soil is a highly non-linear material whose strength and stiffness depends on stress and strain levels. Numerous constitutive models have been developed to simulate the most important features of soil behaviour [1, 2, 3] although there is no agreement on which is the best to model a particular type of soil. The choice of the model rests on the available soil information and the particular design situation. In addition, determination of soil parameters is a difficult task due mainly to the ground heterogeneity, the boundary conditions uncertainty (water table position, layering...), the disturbance suffered by soil specimens during geotechnical sampling and the small quantity of soil surveyed compared to the mass of ground affected by any foundation. Hence, the bulk information yielded by the field surveying and laboratory testing program must be interpreted by an experienced engineer, adding more uncertainty to the choice of the constitutive model and its parameters [4]. In order to ascertain the parameter validity, it is common in geotechnical engineering to perform back analysis or inverse analysis procedures from field instrumentation. The field observations might not be as precise as desired due to the hard site conditions.

*ESET Universidad CEU Cardenal Herrera
†Arup Geotechnics
‡ICITECH Universitat Politècnica de València

Hence, to solve a geotechnical inverse problem means to estimate partially known parameters from indirect noisy observations. This is not an academic issue since it has practical applications, for instance, the information recorded during the early stages of the construction might be used to update and validate the initial design predictions. The back analysis is a tool which enables to gain insight and to understand better the soil-structure system behaviour [5].

Inverse problem resolution is not new since numerous authors have studied it previously [6, 7, 8, 9, 10, 11, 12, 13, 14, 15, 16]. Many of those studies [6, 8, 9, 10, 11, 14] address the back analysis as an optimization problem (i.e. obtaining the set of parameters which minimize an objective function). That approach leads to estimated parameters which reliability is generally unknown [15]. As the model might not be able to reproduce perfectly the actual response and the observations might suffer measurement errors, the solution should take into account the model and observations uncertainties. For that reason, the Bayesian approach is the appropriate methodology to solve inverse problems [17, 18]. In geotechnical engineering, the solution of statistical inverse problems can be a computationally intensive task. The numerical burden arises mainly in two ways [19]: (i) the large number of parameters that the model might require and (ii) the computational cost that might require to run of a single realization.

The main objective of this paper is to present a Bayesian methodology to determine at low numerical expense the model parameters from the observed response at one construction stage of a deep excavation. To that end, the Bayesian methodology is briefly outlined in the first part of this paper. The Bayesian methods regard the model parameters as random variables which are updated once a set of observations are known. As the solution of the problem is posed in terms of random variables, the stochastic spectral representation can be used to reduce the numerical burden [20, 21]. The random variable spectral representation is the backbone of the non-intrusive stochastic finite element methods (SFEM) [22, 23] and hence those methods are briefly described. Once the theoretical framework has been established, the proposed methodology to solve inverse problems is adequately presented. The spectral approach raises two benefits (i) the substantial reduction of computational cost when performing the optimization calculations on the surrogate model constructed by means of SFEM and (ii) the possibility of an analytical computation of the statistical relationship between the different observations (i.e. the covariance matrix). However, the surrogation brings a modelling error affecting the solution. One of the main findings of this paper is the algorithm developed to estimate the surrogation error at low numerical expense. Finally, the proposed methodology is validated by the study of three calibration problems of increasing complexity.

2 Inverse problem solution

The connection between the parameters $\mathbf{m}$ and the observations $\mathbf{d}$ defines the following deterministic forward or response model $\mathbf{g}(\mathbf{m})$, namely:

$$\mathbf{m} \rightarrow \mathbf{d} = \mathbf{g}(\mathbf{m}). \tag{1}$$

The predicted values cannot be identical in general to the observed values due to observational and modelling errors. The goal of the inverse problem is to infer the N model parameters $\mathbf{m}$ from a set of n imperfect observations $\mathbf{d}$. In the Bayesian approach, $\mathbf{m}$ and $\mathbf{d}$ are vectors of random variables. $\rho_d(\mathbf{d})$ is the probability density function (pdf) of the observations and $\rho_m(\mathbf{m})$ encodes any available prior knowledge about the inputs. The key point of Bayesian inference is the way that the *a priori* distribution $\rho_m(\mathbf{m})$ is updated to the *a posteriori* distribution $\sigma_m(\mathbf{m})$ once a set of observations $\mathbf{d}_{obs}$ is known.

The difference between the observed values $\mathbf{d}_{obs}$ and the actual response $\mathbf{d}$ is the observational error. The vector of n residuals $\boldsymbol{\varepsilon}_D$ is regarded in this paper Gaussian of zero mean:

$$\boldsymbol{\varepsilon}_D = \mathbf{d} - \mathbf{d}_{\text{obs}} \sim \text{N}(\mathbf{0}, \mathbf{C}_D), \tag{2}$$

where the covariance matrix $\mathbf{C}_D$ measures the size of those residuals and gives the dependence between them. The *a priori* observation distribution can be written as [24]:

$$\rho_d(\mathbf{d}) \propto \exp\left[-\frac{1}{2}(\mathbf{d} - \mathbf{d}_{\text{obs}})^T \mathbf{C}_D^{-1}(\mathbf{d} - \mathbf{d}_{\text{obs}})\right], \tag{3}$$

As $\mathbf{m}$ and $\mathbf{d}$ are regarded independent random variables, the joint pdf is given by (see Figure 1a):

$$\rho(\mathbf{d}, \mathbf{m}) = \rho_d(\mathbf{d})\rho_m(\mathbf{m}) \tag{4}$$

If the forward model $\mathbf{g}(\mathbf{m})$ were perfect (i.e. modelling errors free), each parameter vector would yield only one observation vector. Nevertheless, most often, the underlying physical theory lacks of some fundamental knowledge or fails to achieve a perfect parametrization [17]. Therefore, the joint probability density $\Theta(\mathbf{d}, \mathbf{m})$ is required to describe the correlations that correspond to the physical theory, together with the inherent uncertainties of the theory (see Figure 1b).

The modelling residual vector is the difference between the model $\mathbf{g}_{real}$ (perfect but unknown) and the available forward model $\mathbf{g}(\mathbf{m})$ (known but imperfect). Again, that residual is assumed in this paper as an additive Gaussian of zero mean:

$$\begin{aligned} \boldsymbol{\varepsilon}_G(\mathbf{m}) &= \mathbf{g}_{real} - \mathbf{g}(\mathbf{m}) \\ \boldsymbol{\varepsilon}_G &\sim \text{N}(\mathbf{0}, \mathbf{C}_G) \end{aligned} \tag{5}$$

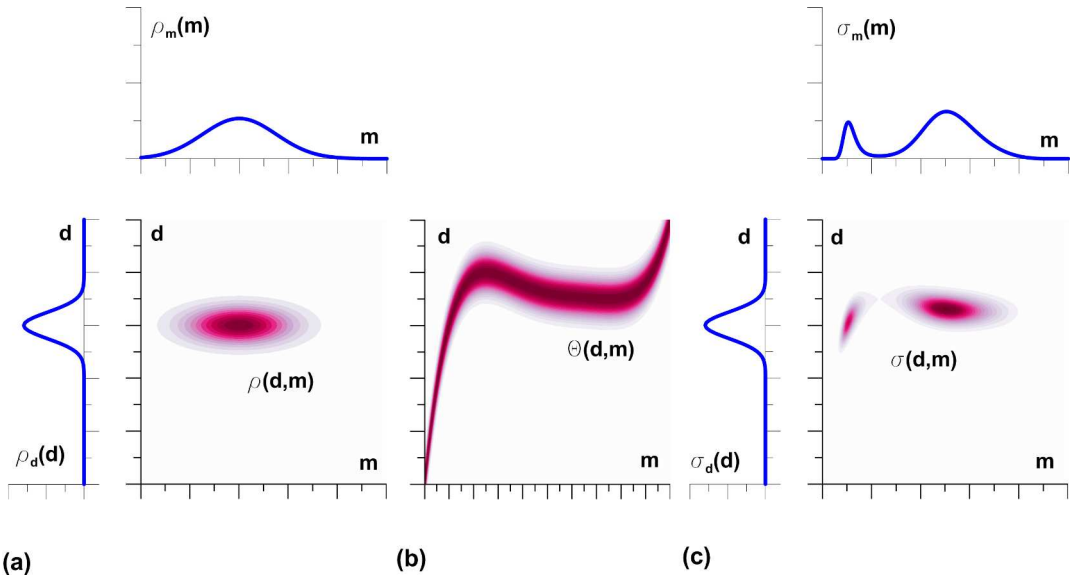

Figure 1: Inverse problem resolution (a) *a priori* parameter and observation marginals, $\rho_m(\mathbf{m})$ and $\rho_d(\mathbf{d})$ respectively, and joint probability functions, $\rho(\mathbf{d},\mathbf{m})$, (b) model joint pdf, $\Theta(\mathbf{d},\mathbf{m})$, (c) *a posteriori* parameter and observation joint pdf, $\sigma(\mathbf{d},\mathbf{m})$, and the *a posteriori* marginal parameter probability distribution function (pdf), $\sigma_m(\mathbf{m})$ (adapted from [17])

where $\mathbf{C}_G$ is the model covariance matrix giving information about the size of the residuals and the correlation between them. The matrix $\mathbf{C}_G$ could be regarded as the model epistemic error and expert judgement is required to estimate it. When the dependence of $\mathbf{d}$ on $\mathbf{m}$ is mildly non-linear, $\Theta(\mathbf{d},\mathbf{m})$ can be expressed as [17]:

$$\Theta\left(\mathbf{d},\mathbf{m}\right) \propto \exp\left[-\frac{1}{2}(\mathbf{g}(\mathbf{m})-\mathbf{d})^T\mathbf{C}_G^{-1}(\mathbf{g}(\mathbf{m})-\mathbf{d})\right]. \tag{6}$$

The conjunction of the information contained in $\rho(\mathbf{d},\mathbf{m})$ and $\Theta(\mathbf{d},\mathbf{m})$ results in the updated or posterior probability density function. The solution of the inverse problem is a new or *a posteriori* pdf $\sigma_m(\mathbf{m})$ which incorporates the information given by the observed values $\mathbf{d}_{obs}$ and it is consistent with the amount of modelling and observational uncertainty [17] (see Figure 1c):

$$\sigma_m(\mathbf{m}) \propto \rho_m(\mathbf{m}) \exp\left[-\frac{1}{2}(\mathbf{d}_{\text{obs}}-\mathbf{g}(\mathbf{m}))^T\left[\mathbf{C}_{\text{G}}+\mathbf{C}_{\text{D}}\right]^{-1}(\mathbf{d}_{\text{obs}}-\mathbf{g}(\mathbf{m}))\right]. \tag{7}$$

3 Stochastic Finite Element Methods (SFEM)

The deterministic finite element method (FEM) yields one solution from a set of known parameters. The deterministic approach to a problem cannot cope rigorously with the intrinsic uncertainty of loads and material properties [25]. Hence, uncertainty is taken roughly into account by means of safety factors which might factorize either response or parameters. If the loading and material properties could be expressed as probability distribution functions, the solution of the model should be given in the same terms. The stochastic finite element methods (SFEM) [22, 25, 20, 23] allow the propagation of these uncertainties throughout the model. The SFEM can be used

seamlessly with the Bayesian approach because both techniques regard the model parameters as random variables. The SFEM are divided into two groups: intrusive and non-intrusive methods.

The intrusive methods are based on the solution of the system of governing equations for the spectral coefficients in the polynomial chaos representation [22, 23]. Hence, an adaptation of the existing software is required in this approach.

The non-intrusive strategy is based in creating a response surface, which depends on the model random parameters, so that a surrogate of the original forward model can be built up. In this paper, a non-intrusive spectral projection method is embraced because it can tackle with non-linear models and any FEM software can be used. As the parameters $\mathbf{m} = (m_1, \ldots, m_N)$ are regarded random variables, a term $g_i(\mathbf{m})$ of the vector $\mathbf{g}(\mathbf{m}) = (g_1(\mathbf{m}), \ldots, g_n(\mathbf{m}))$ is also a random variable. Recall that $g_i(\mathbf{m})$ is a random variable where the variance of $g_i(\mathbf{m})$ is finite, that is, $\operatorname{var} g_i(\mathbf{m}) < \infty$. The variance of $g_i(\mathbf{m})$ is defined as $\operatorname{var} g_i(\mathbf{m}) = \mathrm{E}[(g_i(\mathbf{m}) - \mathrm{E}[g_i(\mathbf{m})])^2]$, where $\mathrm{E}[\bullet]$ denotes the expectation operator. After normalizing m_j to ξ_j, the forward model can be expressed as an infinite Fourier-type expansion:

$$g_i(\mathbf{m}) = s_i(\boldsymbol{\xi}) = \sum_{j=0}^{\infty} u_{ij} \Psi_j(\xi_1, ..., \xi_N), \tag{8}$$

where the functionals $\Psi_j(\boldsymbol{\xi})$ are the so-called chaotic polynomials [22, 20], here $\boldsymbol{\xi} = (\xi_1, \ldots, \xi_N)$, and u_k are the expansion coefficients. The set $\{\Psi_k\}_{k \in \mathbb{N}}$ is known as a multidimensional polynomial chaos (PC) basis [23] and expression (8) is called the spectral representation of $g_i(\mathbf{m})$. This spectral stochastic framework is based on Wiener's [26] ideas of homogeneous chaos which were developed later by Ghanem and Spanos [22]. The variable $g_i(\mathbf{m})$ is an element of an infinite dimensional space (polynomial chaos) which randomness is accounted by $\boldsymbol{\xi}$. Each member of the multidimensional PC basis Ψ_k can be written as a product of the appropriate one-dimensional polynomials ψ_i of the corresponding random variable [23, 20]:

$$\Psi_k(\xi_1, \xi_2, ..., \xi_N) = \prod_{i=1}^{N} \psi_{\alpha_i^k}(\xi_i), \tag{9}$$

where $\alpha_i^k \in \mathbb{Z}_+$ denotes the order of the one-dimensional polynomial in ξ_k and it can be seen as an element of a multi-index $\boldsymbol{\alpha}^k = (\alpha_1^k, \ldots, \alpha_N^k) \in \mathbb{Z}_+^N$. Henceforth, we will identify k with $\boldsymbol{\alpha}^k$ such that $k \leq k'$ if and only if $\boldsymbol{\alpha}^k \leq \boldsymbol{\alpha}^{k'}$ where we consider in $\mathbb{Z}_+^N$ the lexicographical order. In particular, for $k = 0$ we have $\boldsymbol{\alpha}^0 = \mathbf{0}$ and hence $\Psi_0(\boldsymbol{\xi})$ is a constant function. Moreover, by using tensorial notation we can write expression (9) as:

$$\Psi_k = \bigotimes_{i=1}^{N} \psi_{\alpha_i^k} \tag{10}$$

Let $\delta_{m,n}$ denote the Kronecker delta, that is, $\delta_{m,n} = 0$ if and only if $n \neq m$, otherwise $\delta_{n,n} = 1$. The unidimensional

functions, ψ_m, satisfy:

$$\mathrm{E}[\psi_m \cdot \psi_n] \propto \delta_{mn}, \tag{11}$$

for all m, n and hence they are orthogonal polynomial functions. Assuming that $\boldsymbol{\xi}$ is a random vector of independent and identically distributed random variables then, by using tensorial notation, we have:

$$\mathrm{E}[\Psi_k \cdot \Psi_l] = \mathrm{E}\left[\bigotimes_{i=1}^{N} \psi_{\alpha_i^k} \bigotimes_{l=1}^{N} \psi_{\alpha_i^l}\right] = \mathrm{E}\left[\bigotimes_{i=1}^{N} \psi_{\alpha_i^k} \psi_{\alpha_i^l}\right] = \prod_{i=1}^{N} \mathrm{E}\left[\psi_{\alpha_i^k} \psi_{\alpha_i^l}\right] \propto \prod_{i=1}^{N} \delta_{\alpha_i^k, \alpha_i^l} = \delta_{\boldsymbol{\alpha}^k, \boldsymbol{\alpha}^l} \tag{12}$$

There is a correspondence between the type of generalized polynomial chaos ψ_m, and their underlying random variable ξ as shown in Table 1 [27, 20]. The partial tensorization of the multidimensional polynomial chaos basis and its orthogonality simplifies greatly the procedure of statistical calculations. For practical purposes, expression (8) must be truncated up to a certain polynomial degree $\mathfrak{p}$:

$$\begin{aligned} s_i(\boldsymbol{\xi}) &= \sum_{j=0}^{P} u_{ij} \Psi_j(\xi_1, ..., \xi_N) + \sum_{k=P+1}^{\infty} u_{ik} \Psi_k(\xi_1, ..., \xi_N) \\ &= \tilde{s}_i(\boldsymbol{\xi}) + \varepsilon_{T_i}(\boldsymbol{\xi}) \approx \tilde{s}_i(\boldsymbol{\xi}). \end{aligned} \tag{13}$$

The number of components of the truncated series $\tilde{s}_i(\boldsymbol{\xi})$ is given by:

$$P + 1 = \begin{pmatrix} N + \mathfrak{p} \\ \mathfrak{p} \end{pmatrix} = \frac{(N + \mathfrak{p})!}{N! \mathfrak{p}!} \tag{14}$$

We remark that from (13) it is known that $\tilde{s}_i(\boldsymbol{\xi}) \in \mathrm{span}\{\Psi_j : j = 0, \ldots, P\}$ and the truncation error $\varepsilon_{T_i}(\boldsymbol{\xi})$ belongs to orthogonal complement of the linear subspace $\mathrm{span}\{\Psi_j : j = 0, \ldots, P\}$. Then, from expressions (9) and (11) the covariance must meet:

$$\mathrm{cov}\left[\tilde{s}_i, \varepsilon_{T_j}\right] = 0, \tag{15}$$

for all i and j. The covariance is defined as $\mathrm{cov}\left[\tilde{s}_i, \varepsilon_{T_j}\right] = \mathrm{E}[(\tilde{s}_i - \mathrm{E}[\tilde{s}_i])(\varepsilon_{T_j} - \mathrm{E}[\varepsilon_{T_j}])]$.

The non-intrusive SFEM replaces the original model $g_i(\mathbf{m})$ by a N-dimensional surface built with orthogonal polynomials $\tilde{s}_i(\boldsymbol{\xi})$. That surface might be regarded as a surrogate of the forward model, a sort of vademecum that includes all solutions for every possible value of the parameters. The spectral representation enables (i) the reduction of the computational burden (the evaluation of a polynomial might take far less than the original forward model) and (ii) the disclosure of the statistical structure of the observations as shown below.

The expansion coefficients u_{ij} in equation (13) are computed from realizations of the original forward model. Thus, the original model is a sort of black box which generates information to construct the response surface. Among the different non-intrusive techniques [23], the least squares fit is adopted in this paper because the number of realizations required to determine the expansion coefficients is lower than the other available techniques [28].

Distribution of ξ	PC basis polynomials	Support
Gaussian	Hermite	$(-\infty, \infty)$
Gamma	Laguerre	$[0, \infty)$
Beta	Jacobi	$[a, b]$
Uniform	Legendre	$[a, b]$
Poisson	Charlier	$\{0, 1, 2, \ldots\}$
Binomial	Krawtchouk	$\{0, 1, \ldots, N\}$
Negative binomial	Meixner	$\{0, 1, 2, \ldots\}$
Hypergeometric	Hahn	$\{0, 1, \ldots, N\}$

Table 1: Correspondence between the type of generalized polynomial chaos and their underlying random variables [20]

Sudret's [29] technique to calculate the expansion coefficients is used in this paper.

4 Methodology

Once an (i) *a priori* statistical estimation of the parameters $\rho_m(\mathbf{m})$ is established, (ii) the model uncertainty (after some judgement) is encoded in the covariance matrix $\mathbf{C}_G$ and (iii) the vector of observations $\mathbf{d}_{obs}$ and its covariance matrix $\mathbf{C}_D$ are known, the *a posteriori* parameter joint pdf $\sigma_m(\mathbf{m})$ which is the solution of the inverse problem is given by expression (7). If the original forward model model $\mathbf{g}(\mathbf{m})$ is computationally heavy, the computation of the parameter marginal distributions, the maximum likelihood point or any other statistical measure of interest might be numerically unfeasible. For those reasons, the truncated expression of $\mathbf{g}(\mathbf{m})$ (equation (13)) might alleviate the numerical needs. The computational burden is minimized using a linear model for each observation expressed in terms of ξ_i:

$$\begin{aligned} g_1(\mathbf{m}) = s_1(\boldsymbol{\xi}) \approx \tilde{s}_1(\boldsymbol{\xi}) = u_{10} + u_{11}\xi_1 + \ldots + u_{1N}\xi_N, \\ \vdots \\ g_n(\mathbf{m}) = s_n(\boldsymbol{\xi}) \approx \tilde{s}_n(\boldsymbol{\xi}) = u_{n0} + u_{n1}\xi_1 + \ldots + u_{nN}\xi_N. \end{aligned} \tag{16}$$

Replacing a term of the original forward model $s_i(\boldsymbol{\xi})$ for a linear surrogate $\tilde{s}_i(\boldsymbol{\xi})$ makes appear a truncation error or residual $\varepsilon_{T_i}(\boldsymbol{\xi})$ which is defined as:

$$\varepsilon_{T_i}(\boldsymbol{\xi}) = s_i(\boldsymbol{\xi}) - \tilde{s}_i(\boldsymbol{\xi}). \tag{17}$$

The truncation residual $\varepsilon_{T_i}(\boldsymbol{\xi})$ is regarded as a modelling error. The matrix $\mathbf{C}_T(\boldsymbol{\xi})$ gives information about the relation between the different residuals and their size (i.e it quantifies the truncation error). Hence, the solution of the problem after the surrogation is:

$$\sigma_{\boldsymbol{\xi}}(\boldsymbol{\xi}) \propto \rho_{\boldsymbol{\xi}}(\boldsymbol{\xi}) \exp\left[-\frac{1}{2}(\mathbf{d}_{obs} - \tilde{\mathbf{s}}(\boldsymbol{\xi}))^T [\mathbf{C}_D + \mathbf{C}_G + \mathbf{C}_T]^{-1} (\mathbf{d}_{obs} - \tilde{\mathbf{s}}(\boldsymbol{\xi}))\right]. \tag{18}$$

Note that equation (18) yields to a less accurate solution than the solution in (7), because it incorporates the

uncertainty rendered by truncation. A higher degree polynomial could be used in order to reduce the truncation error. Nevertheless, the numerical cost of building a higher degree surrogate model might exceed by far the benefits of using a surrogate model. To avoid Markov chain simulations in the characterization of the posterior, El Moselhy and Marzouk [30] propose to construct a map using polynomial expansions that pushes forward the *a priori* to the *a posteriori* distributions. To overcome the difficulties of producing a map using a high degree expansion, those authors propose the use of a sequence of low degree maps to approximate a high degree approximation. In this paper, a similar approach is proposed. The forward direct model $\mathbf{g}(\mathbf{m})$ is approximated by using iteratively low-degree expansions. The iterative strategy has proved to be more effective than using a single high degree polynomial.

As pointed out above, the dependence of $\mathbf{d}$ on $\mathbf{m}$ must be mildly non-linear and, hence low degree expansions should suffice to grasp the main features of the forward model. For that reason, although surrogating the original forward model $\mathbf{g}(\mathbf{m})$ renders a poorer inverse problem solution, the *a posteriori* marginal pdf of each parameter ξ_i can be determined from equation (18) and those marginal distributions can be used to bound the actual solution. If a linear surrogate is used as shown in expression (16), the exponent in equation (18) is a quadratic expression which is easy to integrate numerically to obtain the marginal distributions. The *a posteriori* marginal ξ_i pdf can be used as *a priori* parameter estimation in the next iteration. The process is repeated until the truncation error contained in the covariance matrix $\mathbf{C}_T$ is negligible compared to modelling and observation errors. From a geometrical point of view, the proposed methodology assumes that the hypersurface defined by the forward model $\mathbf{g}(\mathbf{m})$ can be approximated adequately the hyperplane defined by equation (16) in the vicinity of the solution.

In geotechnical engineering, it is difficult to establish a probability distribution for each parameter due to the difficulty of characterizing the soil. For that reason, it is common practice to set a range within the parameter is expected which means statistically to define an uniform pdf. If the parameters are initially defined as ranges, it is proposed to determine the 95% confidence interval from the *a posteriori* marginal ξ_i pdf and construct in the following iteration the new surrogate model using as the new ranges those confidence intervals. Figure 2 depicts the iterative proposed methodology.

4.1 Maximum likelihood point

The maximum likelihood point $\boldsymbol{\xi}^*$ of expression (18) is calculated by solving:

$$\min_{\boldsymbol{\xi}} \left(\mathbf{d}_{obs} - \tilde{\mathbf{s}}\left(\boldsymbol{\xi}\right)\right)^T \left[\mathbf{C}_D + \mathbf{C}_G + \mathbf{C}_T\right]^{-1} \left(\mathbf{d}_{obs} - \tilde{\mathbf{s}}\left(\boldsymbol{\xi}\right)\right) \tag{19}$$

The observations of nearby points usually are highly correlated (e.g. the movements of a concrete diaphragm

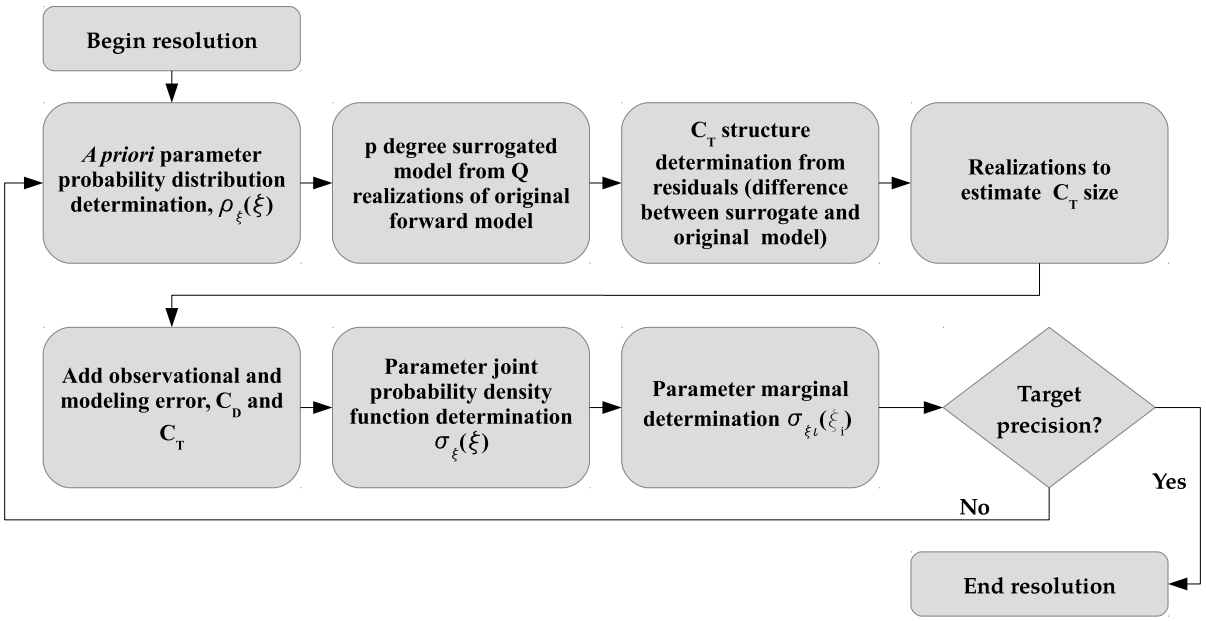

Figure 2: Inverse problem resolution flow chart

wall) and thus the errors. For that reason, the covariance matrix $\mathbf{C}$ might be ill conditioned:

$$\mathbf{C} = \mathbf{C}_D + \mathbf{C}_G + \mathbf{C}_T \tag{20}$$

Since $\mathbf{C}$ is a $n \times n$ positive definite matrix, it can be expressed in term of its eigenvalues:

$$\mathbf{C} = \mathbf{V}_\mathbf{C} \cdot \mathbf{D}_\mathbf{C} \cdot \mathbf{V}_\mathbf{C}^T, \tag{21}$$

where $\mathbf{V}_\mathbf{C}$ is the square matrix whose columns are the $\mathbf{C}$-eigenvectors and $\mathbf{D}_\mathbf{C}$ is the diagonal matrix containing the $\mathbf{C}$-eigenvalues. If the number of observations n is greater than the number of parameters N, the only source of uncertainty are the N model parameter. Hence, only the N higher eigenvalues have got physical meaning and the lower are regarded numerical noise. Performing a principal component analysis, the covariance matrix $\mathbf{C}$ can be approximated using the N higher eigenvalues contained in the diagonal matrix $\tilde{\mathbf{D}}$ and their corresponding eigenvectors $\tilde{\mathbf{V}}_\mathbf{C}$:

$$\mathbf{C} \approx \tilde{\mathbf{V}}_\mathbf{C} \tilde{\mathbf{D}}_\mathbf{C} \tilde{\mathbf{V}}_\mathbf{C}^T. \tag{22}$$

Then the maximum likelihood equation (19) becomes:

$$\min_{\boldsymbol{\xi}} \left[(\mathbf{d}_{obs} - \tilde{\mathbf{s}}(\boldsymbol{\xi}))^T \tilde{\mathbf{V}} \right] \tilde{\mathbf{D}}^{-1} \left[(\mathbf{d}_{obs} - \tilde{\mathbf{s}}(\boldsymbol{\xi}))^T \tilde{\mathbf{V}} \right]^T \tag{23}$$

Now, if the linear model presented in expression (16) is adopted, $\mathbf{d}_{obs} - \tilde{\mathbf{s}}(\boldsymbol{\xi})$ could be written as:

$$\begin{aligned}\mathbf{d}_{obs} - \tilde{\mathbf{s}}(\boldsymbol{\xi}) &= \begin{bmatrix} d_{obs1} - u_{10} & -u_{11} & \cdots & -u_{1N} \\ \vdots & \vdots & \ddots & \vdots \\ d_{obsn} - u_{n0} & -u_{n1} & \cdots & -u_{nN} \end{bmatrix} \begin{bmatrix} 1 \\ \xi_1 \\ \vdots \\ \xi_N \end{bmatrix} \\ &= \begin{bmatrix} b_{10} & b_{11} & \cdots & b_{1N} \\ \vdots & \vdots & \ddots & \vdots \\ b_{n0} & b_{n1} & \cdots & b_{nN} \end{bmatrix} \begin{bmatrix} 1 \\ \boldsymbol{\xi} \end{bmatrix} = \mathbf{M}_{\varepsilon} \begin{bmatrix} 1 & \boldsymbol{\xi} \end{bmatrix}^T \end{aligned} \tag{24}$$

Substituting $\mathbf{d}_{obs} - \tilde{\mathbf{s}}(\boldsymbol{\xi})$ for expression (24) in (23):

$$\begin{aligned}\left[(\mathbf{d}_{obs} - \tilde{\mathbf{s}}(\boldsymbol{\xi}))^T \tilde{\mathbf{V}}\right] \tilde{\mathbf{D}}^{-1} \left[(\mathbf{d}_{obs} - \tilde{\mathbf{s}}(\boldsymbol{\xi}))^T \tilde{\mathbf{V}}\right]^T &= \left[\begin{bmatrix} 1 & \boldsymbol{\xi} \end{bmatrix} \mathbf{M}_{\varepsilon} \mathbf{V}_{\mathbf{C}}\right] \mathbf{D}_{\mathbf{C}}^{-1} \left[\begin{bmatrix} 1 & \boldsymbol{\xi} \end{bmatrix} \mathbf{M}_{\varepsilon} \mathbf{V}_{\mathbf{C}}\right]^T \\ &= \begin{bmatrix} 1 & \boldsymbol{\xi} \end{bmatrix} \mathbf{M}_{\varepsilon} \mathbf{V}_{\mathbf{C}} \mathbf{D}_{\mathbf{C}}^{-1} \mathbf{V}_{\mathbf{C}}^T \mathbf{M}_{\varepsilon}^T \begin{bmatrix} 1 & \boldsymbol{\xi} \end{bmatrix}^T \\ &= \begin{bmatrix} 1 & \boldsymbol{\xi} \end{bmatrix} \begin{bmatrix} h_{00} & h_{01} & \cdots & h_{0N} \\ h_{10} & h_{11} & \cdots & h_{1N} \\ \vdots & \vdots & \ddots & \vdots \\ h_{N0} & h_{N1} & \cdots & h_{NN} \end{bmatrix} \begin{bmatrix} 1 & \boldsymbol{\xi} \end{bmatrix}^T \end{aligned} \tag{25}$$

Hence (19) is equivalent to:

$$\min_{\boldsymbol{\xi}} \begin{bmatrix} 1 & \boldsymbol{\xi} \end{bmatrix} \mathbf{H} \begin{bmatrix} 1 & \boldsymbol{\xi} \end{bmatrix}^T, \tag{26}$$

where $\mathbf{H}$ is a symmetric matrix and thus expression (26) is a quadratic problem which might be efficiently solved [31].

4.2 Surrogate response variance/ covariance closed form

The polynomials $\Psi_k(\boldsymbol{\xi})$ are mutually orthogonal, the truncation error $\varepsilon_{T_i}(\boldsymbol{\xi})$ is an independent random variable of the rest of $\tilde{s}_i(\boldsymbol{\xi})$ as shown in equation (15). Hence, the following relationships must be met:

$$\operatorname{cov}(s_i(\boldsymbol{\xi}), s_j(\boldsymbol{\xi})) = \operatorname{cov}(\tilde{s}_i(\boldsymbol{\xi}), \tilde{s}_j(\boldsymbol{\xi})) + \operatorname{cov}(\varepsilon_{Ti}(\boldsymbol{\xi}), \varepsilon_{Tj}(\boldsymbol{\xi})) \tag{27}$$

Note that $\operatorname{cov}(s_i(\boldsymbol{\xi}), s_i(\boldsymbol{\xi})) = \operatorname{var} s_i(\boldsymbol{\xi})$. Generalising expression (27) to all components of vector $\mathbf{s}(\boldsymbol{\xi})$, the

following relation of covariance matrices can be established:

$$\begin{aligned}
\mathbf{C}_S(\boldsymbol{\xi}) &= \begin{bmatrix} \operatorname{var}(s_1(\boldsymbol{\xi})) & \cdots & \operatorname{cov}(s_1(\boldsymbol{\xi}), s_n(\boldsymbol{\xi})) \\ \vdots & \ddots & \vdots \\ \operatorname{cov}(s_1(\boldsymbol{\xi}), s_n(\boldsymbol{\xi})) & \cdots & \operatorname{var}(s_n(\boldsymbol{\xi})) \end{bmatrix} = \\
&= \begin{bmatrix} \operatorname{var}(\tilde{s}_1(\boldsymbol{\xi})) & \cdots & \operatorname{cov}(\tilde{s}_1(\boldsymbol{\xi}), \tilde{s}_n(\boldsymbol{\xi})) \\ \vdots & \ddots & \vdots \\ \operatorname{cov}(\tilde{s}_1(\boldsymbol{\xi}), \tilde{s}_n(\boldsymbol{\xi})) & \cdots & \operatorname{var}(\tilde{s}_n(\boldsymbol{\xi})) \end{bmatrix} + \begin{bmatrix} \operatorname{var}(\varepsilon_1(\boldsymbol{\xi})) & \cdots & \operatorname{cov}(\varepsilon_1(\boldsymbol{\xi}), \varepsilon_n(\boldsymbol{\xi})) \\ \vdots & \ddots & \vdots \\ \operatorname{cov}(\varepsilon_1(\boldsymbol{\xi}), \varepsilon_n(\boldsymbol{\xi})) & \cdots & \operatorname{var}(\varepsilon_n(\boldsymbol{\xi})) \end{bmatrix} \\
&= \mathbf{C}_{\widetilde{S}}(\boldsymbol{\xi}) + \mathbf{C}_T(\boldsymbol{\xi}),
\end{aligned} \tag{28}$$

where $\mathbf{C}_S(\boldsymbol{\xi})$ is the $n \times n$ covariance matrix of the different random responses given by the normalized forward model $\mathbf{s}(\boldsymbol{\xi})$, $\mathbf{C}_{\widetilde{S}}(\boldsymbol{\xi})$ is the covariance matrix of the surrogate model $\tilde{\mathbf{s}}(\boldsymbol{\xi})$ and $\mathbf{C}_T(\boldsymbol{\xi})$ is the truncation residual covariance matrix. Those matrices are depending on the $\boldsymbol{\xi}$ pdf distribution.

A surrogate $\tilde{s}_i(\boldsymbol{\xi})$ of the forward model $s_i(\boldsymbol{\xi})$ can be written in terms of multidimensional chaotic polynomials which are constructed of unidimensional chaotic polynomials (9):

$$\tilde{s}_i(\boldsymbol{\xi}) = \sum_{j=0}^{P} u_{ij} \Psi_j(\boldsymbol{\xi}) = \sum_{j=0}^{P} u_{ij} \prod_{m=1}^{N} \psi_{\alpha_m^j}(\xi_m) \tag{29}$$

An advantage of the spectral representation is that the variance of $\tilde{s}_i(\boldsymbol{\xi})$ and the covariance between $\tilde{s}_j(\boldsymbol{\xi})$ and $\tilde{s}_k(\boldsymbol{\xi})$ can be calculated analytically saving a lot of computational resources as no Monte Carlo methods [32] are required. Furthermore, obtaining the surrogate covariance matrix $\mathbf{C}_{\widetilde{S}}(\boldsymbol{\xi})$ discloses the statistical structure of the surrogated model.

Since the chaotic polynomials are mutually orthogonal (11), the expectation of any response $\mathrm{E}[\tilde{s}_i(\boldsymbol{\xi})]$ is the independent term:

$$\mathrm{E}[\tilde{s}_i(\boldsymbol{\xi})] = u_{i0} \tag{30}$$

By using the definition of variance:

$$\begin{aligned}
\operatorname{var}[\tilde{s}_i(\boldsymbol{\xi})] &= \mathrm{E}\left((\tilde{s}_i(\boldsymbol{\xi}) - \mathrm{E}[\tilde{s}_i(\boldsymbol{\xi})])^2\right) = \mathrm{E}\left([\tilde{s}_i(\boldsymbol{\xi}) - u_{i0}]^2\right) \\
&= \mathrm{E}\left([\tilde{s}_i(\boldsymbol{\xi})]^2\right) - 2u_{i0}\mathrm{E}(\tilde{s}_i(\boldsymbol{\xi})) + u_{i0}^2 \\
&= \mathrm{E}\left([\tilde{s}_i(\boldsymbol{\xi})]^2\right) - u_{i0}^2 \\
&= \mathrm{E}\left(\left[\sum_{k=0}^{P} u_{ik} \prod_{m=1}^{N} \psi_{\alpha_m^k}(\xi_m)\right]\left[\sum_{l=0}^{P} u_{il} \prod_{n=1}^{N} \psi_{\alpha_n^l}(\xi_n)\right]\right) - u_{i0}^2
\end{aligned} \tag{31}$$

The chaotic polynomial orthogonality imposes that value of the latter product is not nil in the products where $\boldsymbol{\alpha}^k = \boldsymbol{\alpha}^l$ (12) and hence:

$$\operatorname{var}\left[\tilde{s}_i\left(\boldsymbol{\xi}\right)\right] = \sum_{k=0}^{P} u_{ik}^2 \mathrm{E}\left(\prod_{m=1}^{N} \psi_{\alpha_m^k}^2\left(\xi_m\right)\right) - u_{i0}^2 \tag{32}$$

The covariance between $\tilde{s}_i\left(\boldsymbol{\xi}\right)$ and $\tilde{s}_j\left(\boldsymbol{\xi}\right)$ can be similarly obtained:

$$\operatorname{cov}\left[\tilde{s}_i\left(\boldsymbol{\xi}\right), \tilde{s}_j\left(\boldsymbol{\xi}\right)\right] = \sum_{k=0}^{P} u_{ik} u_{jk} \mathrm{E}\left(\prod_{m=1}^{N} \psi_{\alpha_m^k}^2\left(\xi_m\right)\right) - u_{i0} \cdot u_{j0} \tag{33}$$

4.3 Variance sensitivity analysis

The variance of a multidimensional chaotic polynomial can be obtained from the variances of the unidimensional chaotic polynomials:

$$\begin{aligned} \operatorname{var}\left(\Psi_k\left(\boldsymbol{\xi}\right)\right) &= \mathrm{E}\left(\left[\prod_{m=1}^{N} \psi_{\alpha_m^k}^2\left(\xi_m\right)\right]\right) \\ &= \int \psi_{\alpha_1^k}^2\left(\xi_1\right) f_{\xi_1}\left(\xi_1\right) d\xi_1 \cdots \int \psi_{\alpha_N^k}^2\left(\xi_N\right) f_{\xi_N}\left(\xi_N\right) d\xi_N \\ &= \operatorname{var}\left(\psi_{\alpha_1^k}\left(\xi_1\right)\right) \cdots \operatorname{var}\left(\psi_{\alpha_N^k}\left(\xi_N\right)\right) \end{aligned} \tag{34}$$

Taking logarithms in expression (34), the product turns up into a sum:

$$\begin{aligned} \log\left[\operatorname{var}\left(\Psi_k\left(\boldsymbol{\xi}\right)\right)\right] &= \log\left[E\left(\left[\prod_{m=1}^{N} \psi_{\alpha_m^k}^2\left(\xi_m\right)\right]\right)\right] \\ &= \log\left[\operatorname{var}\left(\psi_{\alpha_1^k}\left(\xi_1\right)\right) \cdots \operatorname{var}\left(\psi_{\alpha_N^k}\left(\xi_N\right)\right)\right] \\ &= \log\left[\operatorname{var}\left(\psi_{\alpha_1^k}\left(\xi_1\right)\right)\right] + \cdots + \log\left[\operatorname{var}\left(\psi_{\alpha_N^k}\left(\xi_N\right)\right)\right], \end{aligned} \tag{35}$$

and hence the following equation holds:

$$1 = \frac{\log\left[\operatorname{var}\left(\psi_{\alpha_1^k}\left(\xi_1\right)\right)\right]}{\log\left[\operatorname{var}\left(\Psi_k\left(\boldsymbol{\xi}\right)\right)\right]} + \cdots + \frac{\log\left[\operatorname{var}\left(\psi_{\alpha_N^k}\left(\xi_N\right)\right)\right]}{\log\left[\operatorname{var}\left(\Psi_k\left(\boldsymbol{\xi}\right)\right)\right]} \tag{36}$$

Multiplying the latter expression by $\operatorname{var}\left(\Psi_k\left(\boldsymbol{\xi}\right)\right)$:

$$\operatorname{var}\left(\Psi_k\left(\boldsymbol{\xi}\right)\right) = \log\left[\operatorname{var}\left(\psi_{\alpha_1^k}\left(\xi_1\right)\right)\right] \frac{\operatorname{var}\left(\Psi_k\left(\boldsymbol{\xi}\right)\right)}{\log\left[\operatorname{var}\left(\Psi_k\left(\boldsymbol{\xi}\right)\right)\right]} + \cdots + \log\left[\operatorname{var}\left(\psi_{\alpha_N^k}\left(\xi_N\right)\right)\right] \frac{\operatorname{var}\left(\Psi_k\left(\boldsymbol{\xi}\right)\right)}{\log\left[\operatorname{var}\left(\Psi_k\left(\boldsymbol{\xi}\right)\right)\right]} \tag{37}$$

Then the coefficient $\varphi_k(\xi_i) := \log\left[\operatorname{var}\left(\psi_{\alpha_i^k}\left(\xi_i\right)\right)\right] / \log\left[\operatorname{var}\left(\Psi_k\left(\boldsymbol{\xi}\right)\right)\right]$ might be considered as the influence of the random variable ξ_i in the variance of $\operatorname{var}\left(\Psi_k\left(\boldsymbol{\xi}\right)\right)$. From equations (33) and (37), the covariance matrix $\tilde{\mathbf{C}}_{\mathbf{S}}$ can be decomposed into the sum of the "covariance" matrices of each parameter:

$$\tilde{\mathbf{C}}_{\mathbf{S}} = \tilde{\mathbf{C}}_{\mathbf{S}}^{\xi_1} + \cdots + \tilde{\mathbf{C}}_{\mathbf{S}}^{\xi_N} \tag{38}$$

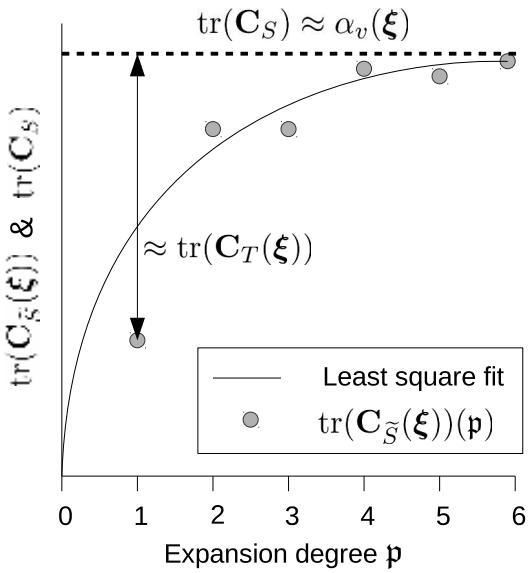

Figure 3: Surrogate model variance evolution in relation to the expansion polynomial degree $\mathfrak{p}$

The latter decomposition of $\tilde{\mathbf{C}}_{\mathbf{S}}$ is a sensitivity analysis because the influence of $\boldsymbol{\xi}$ on the total variance is analytically determined.

4.4 The Truncation error

The trace of the covariance matrices is an invariant. Hence, from expression (28), the following relation can be derived:

$$\mathrm{tr}(\mathbf{C}_S(\boldsymbol{\xi})) = \mathrm{tr}(\mathbf{C}_{\widetilde{S}}(\boldsymbol{\xi})) + \mathrm{tr}(\mathbf{C}_T(\boldsymbol{\xi})), \tag{39}$$

where tr denotes the usual trace matrix operator. $\mathbf{C}_{\widetilde{S}}(\boldsymbol{\xi})$ can be obtained analytically as shown previously and the estimation of $\mathrm{tr}(\mathbf{C}_T(\boldsymbol{\xi}))$, which is a measure of the truncation error, would require simply the determination of $\mathrm{tr}(\mathbf{C}_S(\boldsymbol{\xi}))$. The problem is that the computation of $\mathbf{C}_S(\boldsymbol{\xi})$ might require the evaluation of thousands times the forward model at great numerical expense. The challenge is to obtain an estimation of $\mathbf{C}_T(\boldsymbol{\xi})$ running the least number of times the forward model. If Q realizations of the forward model have been required to build the the surrogate model, $n \times Q$ residuals can be used to calculate the sample covariance matrix $\hat{\mathbf{C}}_T(\boldsymbol{\xi})$. It has been observed that $\hat{\mathbf{C}}_T(\boldsymbol{\xi})$ grasps properly the structure of $\mathbf{C}_T(\boldsymbol{\xi})$ (i.e. correlation between the different truncation residuals) but it fails to estimate the size of the error (norm of matrix $\mathbf{C}_T(\boldsymbol{\xi})$). That is due to the least square fit chosen to determine the expansion coefficients.

Equation (14) is a combinatorial expression and, when the expansion degree $\mathfrak{p}$ increases, the number of terms increases in a pseudo-exponential way. Furthermore, expression (8) converges in quadratical mean [22]. For those reasons, it is assumed that $\mathrm{tr}(\mathbf{C}_{\widetilde{S}}(\boldsymbol{\xi}))$ could be fitted exponentially (see Figure 3) as the expansion degree $\mathfrak{p}$

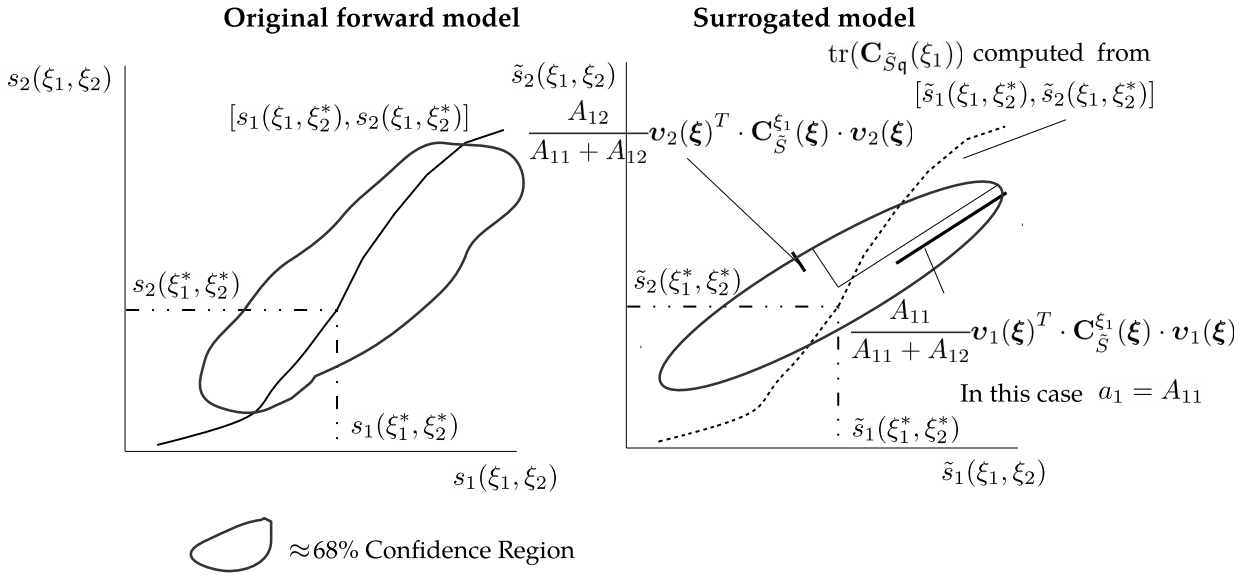

Figure 4: Graphical description of the truncation error estimation (just two variables and observations have been considered for clarity)

increases:

$$\mathrm{tr}(\mathbf{C}_{\widetilde{S}}(\boldsymbol{\xi}))(\mathfrak{p}) \approx \alpha_v(\boldsymbol{\xi})(1-\mathrm{e}^{-\alpha_\varepsilon(\boldsymbol{\xi})\cdot\mathfrak{p}}), \tag{40}$$

where $\alpha_v(\boldsymbol{\xi})$ and $\alpha_\varepsilon(\boldsymbol{\xi})$ are the fitting coefficients. When $\mathfrak{p}\to\infty$, $\mathrm{tr}(\mathbf{C}_{\widetilde{S}}(\boldsymbol{\xi}))(\mathfrak{p}) \to \mathrm{tr}(\mathbf{C}_S(\boldsymbol{\xi}))$. Hence, the coefficient $\alpha_v(\boldsymbol{\xi})$ can be seen as an approximation of $\mathrm{tr}(\mathbf{C}_S(\boldsymbol{\xi}))$.

From equation (40), parameters $\alpha_v(\boldsymbol{\xi})$ and $\alpha_\varepsilon(\boldsymbol{\xi})$ could be determined computing $\mathrm{tr}(\mathbf{C}_{\widetilde{S}}(\boldsymbol{\xi}))(\mathfrak{p}=1)$ and $\mathrm{tr}(\mathbf{C}_{\widetilde{S}}(\boldsymbol{\xi}))(\mathfrak{p}=2)$. Nevertheless, that method suffers from two weaknesses (i) if the number of parameters is high, even the evaluation of the surrogate model for $\mathfrak{p}=2$ could be numerically unfeasible and (ii) as a least square fit which requires a low number of realizations of the forward model is used, it has been observed that the variance estimation for low degree expansions is not very accurate. For those reasons, a method to estimate the residual error which takes advantage of (i) the possibility of evaluating the contribution of each variable in the overall variance as shown above and (ii) the fact that the numerical cost of generating very high degree unidimensional surrogate models is affordable. The method, which is graphically described in Figure 4, takes the following steps:

1. The covariance matrix $\mathbf{C}_{\widetilde{S}}(\boldsymbol{\xi})$, as shown previously, can be decomposed into a sum of "covariance" matrices depending of each parameter:

$$\mathbf{C}_{\widetilde{S}}(\boldsymbol{\xi}) = \mathbf{C}_{\widetilde{S}}^{\xi_1}(\boldsymbol{\xi}) + \cdots + \mathbf{C}_{\widetilde{S}}^{\xi_N}(\boldsymbol{\xi}). \tag{41}$$

2. As the the covariance matrix $\mathbf{C}_{\widetilde{S}}(\boldsymbol{\xi})$ is a positive definite matrix, the eigenvalues $\lambda_i(\boldsymbol{\xi})$ and the corresponding

eigenvectors $\boldsymbol{v}_i(\boldsymbol{\xi})$ can be easily computed. Then:

$$\mathrm{tr}(\mathbf{C}_{\widetilde{S}}(\boldsymbol{\xi})) = \sum_j \lambda_j(\boldsymbol{\xi}) = \sum_j \boldsymbol{v}_j(\boldsymbol{\xi})^T \cdot \mathbf{C}_{\widetilde{S}}(\boldsymbol{\xi}) \cdot \boldsymbol{v}_j(\boldsymbol{\xi}) = \sum_j \sum_i \boldsymbol{v}_j(\boldsymbol{\xi})^T \cdot \mathbf{C}_{\widetilde{S}}^{\xi_i}(\boldsymbol{\xi}) \cdot \boldsymbol{v}_j(\boldsymbol{\xi}). \tag{42}$$

Thus $\mathrm{tr}(\mathbf{C}_{\widetilde{S}}(\boldsymbol{\xi}))$ can be constructed by equation (42) and, since $\mathrm{tr}(\mathbf{C}_{\widetilde{S}}(\boldsymbol{\xi})) = \sum_i \mathrm{tr}(\mathbf{C}_{\widetilde{S}}^{\xi_i}(\boldsymbol{\xi}))$, we can deduce that $\mathrm{tr}(\mathbf{C}_{\widetilde{S}}^{\xi_i}(\boldsymbol{\xi})) = \sum_j \boldsymbol{v}_j(\boldsymbol{\xi})^T \cdot \mathbf{C}_{\widetilde{S}}^{\xi_i}(\boldsymbol{\xi}) \cdot \boldsymbol{v}_j(\boldsymbol{\xi})$. Moreover, $\boldsymbol{v}_j(\boldsymbol{\xi})^T \cdot \mathbf{C}_{\widetilde{S}}^{\xi_i}(\boldsymbol{\xi}) \cdot \boldsymbol{v}_j(\boldsymbol{\xi})$ can be seen as the contribution of the parameter ξ_i over the principal axis defined by the $\boldsymbol{v}_j(\boldsymbol{\xi})$ eigenvector.

3. The computational cost of constructing a one dimensional surrogate model is small even for high degree expansions. Thus, adopting a set of parameters $\boldsymbol{\xi}^*$and fixing to those values all variables except ξ_i,

$$s_j(\xi_1^*, \ldots, \xi_{i-1}^*, \xi_i, \xi_{i+1}^*, \ldots, \xi_N^*) = s_j(\boldsymbol{\xi}^*(\xi_i)) \tag{43}$$

a very good estimation of $s_j(\boldsymbol{\xi}^*(\xi_i))$ can be achieved using $\tilde{s}_{\mathfrak{q},j}(\xi_i)$ which is a $\mathfrak{q}$ degree unidimensional expansion ($\mathfrak{q} \gg \mathfrak{p}$). The following covariance matrix is defined:

$$\mathbf{C}_{\widetilde{S}_{\mathfrak{q}}}(\xi_i) = \begin{bmatrix} \mathrm{var}\left(\tilde{s}_{\mathfrak{q},1}(\xi_i)\right) & \cdots & \mathrm{cov}\left(\tilde{s}_{\mathfrak{q},1}(\xi_i), \tilde{s}_{\mathfrak{q},n}(\xi_i)\right) \\ \vdots & \ddots & \vdots \\ \mathrm{cov}\left(\tilde{s}_{\mathfrak{q},1}(\xi_i), \tilde{s}_{\mathfrak{q},n}(\xi_i)\right) & \cdots & \mathrm{var}\left(\tilde{s}_{\mathfrak{q},n}(\xi_i)\right) \end{bmatrix} \tag{44}$$

4. Let define the matrix $A_{ij} = \boldsymbol{v}_j(\boldsymbol{\xi})^T \cdot \mathbf{C}_{\widetilde{S}}^{\xi_i}\boldsymbol{\xi}) \cdot \boldsymbol{v}_j(\boldsymbol{\xi})$. In order to use $\mathrm{tr}(\mathbf{C}_{\widetilde{S}_{\mathfrak{q}}}(\xi_i))$ in the role of $\mathrm{tr}(\mathbf{C}_{\widetilde{S}}^{\xi_i}(\boldsymbol{\xi}))$, take:

$$a_i(\boldsymbol{\xi}) = \mathrm{max}_j\{A_{ij}\} \tag{45}$$

Next, the value $a_i(\boldsymbol{\xi})$ is compared to $\mathrm{tr}(\mathbf{C}_{\widetilde{S}_{\mathfrak{q}}}(\xi_i))$ for all index i and we proceed as follows. If $\mathrm{tr}(\mathbf{C}_{\widetilde{S}_{\mathfrak{q}}}(\xi_i) \geq a_i(\boldsymbol{\xi})$, we take $\mu_i(\boldsymbol{\xi}) = \mathrm{tr}(\mathbf{C}_{\widetilde{S}_{\mathfrak{q}}}(\xi_i)/a_i(\boldsymbol{\xi})$ otherwise $\mu_i = 1$. Finally, let μ be the average of the set μ_i for all indices i. The trace of the forward model can be approximated:

$$\mathrm{tr}(\mathbf{C}_S(\boldsymbol{\xi})) \approx \mu \cdot \mathrm{tr}(\mathbf{C}_{\widetilde{S}}(\boldsymbol{\xi})) = \mu \cdot \sum_j \lambda_j(\boldsymbol{\xi}) \tag{46}$$

$\mathrm{tr}(\mathbf{C}_{\widetilde{S}}(\boldsymbol{\xi}))$ is a measure of the whole surrogate. Likewise, $\mathrm{tr}(\mathbf{C}_{\widetilde{S}_{\mathfrak{q}}}(\xi_i))$ is a measure of the surrogate variability depending on ξ_i once $\xi_{j\ j\neq i}$ are fixed to $\xi_{j\ j\neq i}^*$. Though $\mathrm{tr}(\mathbf{C}_{\widetilde{S}_{\mathfrak{q}}}(\xi_i))$ being computed from a surrogate model, it is regarded to be very close to the original because a high degree expansion can be attained. The spectral structure of the surrogate response enables to determine the maximum influence a_i of a given variable ξ_i along the different eigenvectors v_i. Hence, it is sensible to expect that $\mathrm{tr}(\mathbf{C}_{\widetilde{S}_{\mathfrak{q}}}(\xi_i))$ must be similar to a_i.

5. Therefore, from (39), the trace of the residual remains as:

$$\mathrm{tr}(\mathbf{C}_T(\boldsymbol{\xi})) \approx (\mu - 1) \cdot \mathrm{tr}(\mathbf{C}_{\widetilde{S}}(\boldsymbol{\xi})). \tag{47}$$

5 Stochastic calibration

The methodology is validated by the resolution of three problems. The first problem is a very simple case because one parameter is determined from one observation linked by an explicit formula and the observation is numerically or synthetically generated. As the "true" solution of the first problem is known, questions such as the effect of running the analysis on a surrogate model can be easily addressed. Furthermore, as only one parameter and one observation are involved in the analysis, graphical resolution can be displayed and ease the understanding of the proposed methodology. The second example is a synthetic excavation where the complexity is increased by determining five parameters from twelve numerically generated observations. The third problem is a well known sheet pile wall field test at Hochstetten (Germany) [33, 34, 35]. The goal of the last case is to identify nine soil parameters from fourteen horizontal wall displacements at the last stage of the excavation. This case is real and we must deal with uncertainty in the model and the observations. It is noted that the performance of the surrogate models (like Bayesian models) is influenced by the input parameters and the sample size.

5.1 Wall Bending stiffness determination (Problem A)

5.1.1 Problem A definition

The aim of this example is to determine the bending stiffness EI of a 4.0 m high wall from its top horizontal displacement. It is assumed that the wall footing and the soil are stiff enough to prevent any rotation of the wall stem base. Hence, the wall stem can be regarded as a cantilever beam carrying a triangular earth pressure, $\sigma_h = K_a \cdot \sigma_v = 0.333 \cdot 4.0 \cdot 20 = 26.64\,\mathrm{kPa}$ as shown in Figure 5. As stated above, the Bayesian methodology requires three ingredients expressed in terms of probability function: (i) the forward or response model, (ii) the observation and (iii) the parameter estimation. The forward model which in this case is the wall deflection is given by the following expression:

$$g(m) = \frac{\sigma_h \cdot l^4}{30 \cdot m} = \frac{227.55}{m} \tag{48}$$

The bending stiffness EI is denoted as m to keep a consistent notation. As the model perfectly describes the observed movement, its probability density function is:

$$\Theta(d, m) = \delta(d - g(m)), \tag{49}$$

Let δ denote the Dirac function, that is $\delta(0) = 1$ and $\delta(x) = 0$ for $x \neq 0$. The observation $d_{obs} = 1.75\,\mathrm{mm}$ is

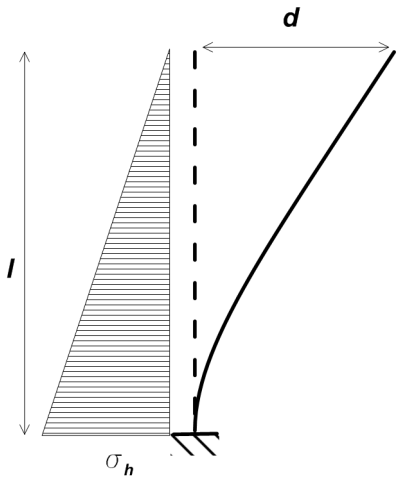

Figure 5: Cantilever model (Problem A)

free of observational error and all the probability of occurrence is concentrated at that value:

$$\rho_d(d) = \delta(d - d_{obs}) \tag{50}$$

It is estimated that the bending stiffness could be a random value between 10^5 and $3.5 \cdot 10^5\,\mathrm{kN \cdot m^2}$. Therefore, the *a priori* parameter distribution is:

$$\rho_m(m) = \begin{cases} \dfrac{1}{3.5 \cdot 10^5 - 10^5} & m \in \left[10^5, 3.5 \cdot 10^5\right] \\ 0 & m \notin \left[10^5, 3.5 \cdot 10^5\right] \end{cases} \tag{51}$$

From a practical point of view, this problem poses no difficulty because, once known d_{obs}, obtaining m from equation (48) is straightforward. Nevertheless, the resolution of this simple problem might be very useful to illustrate the proposed methodology graphically. This problem is solved in two ways: (i) assuming that there are enough computational resources to tackle the original forward model, equation (48), and (ii) considering the forward model is numerically too demanding and a surrogate model is needed to alleviate that burden.

5.1.2 Problem A resolution with original forward model

Combining equations (50) and (51), the *a priori* joint probability density $\rho(d, m)$ is given by:

$$\rho(d, m) = \begin{cases} \dfrac{1}{3.5 \cdot 10^5 - 10^5} & m \in \left[10^5, 3.5 \cdot 10^5\right] \text{ and } d_{obs} = 1.75\,\mathrm{mm} \\ 0 & m \notin \left[10^5, 3.5 \cdot 10^5\right] \text{ or } d_{obs} \neq 1.75\,\mathrm{mm} \end{cases} \tag{52}$$

In Figure 6a, we show that all the probability of occurrence in the parameter and observation space is concentrated in the segment defined by expression (52). Likewise, as shown in figure 6b, equation (49) defines a curve

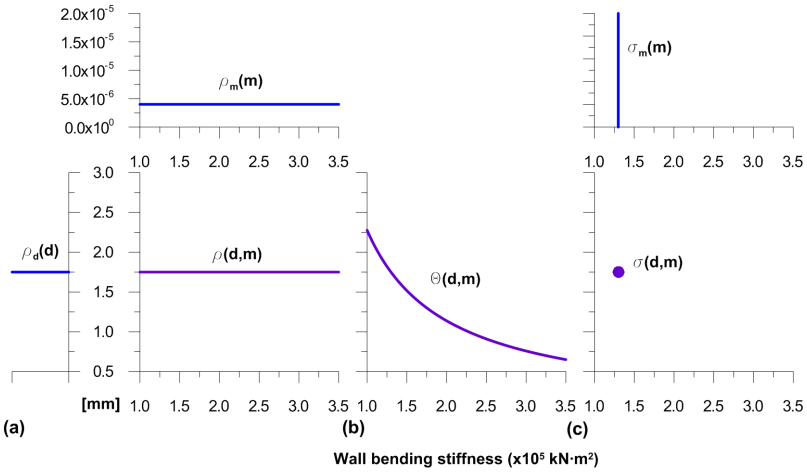

Figure 6: Bayesian resolution of problem A using the original forward model. No modelling or observational uncertainties (a) parameters and observations *a priori* pdf, (b) model pdf and (c) parameters and observations *a posteriori* pdf.

of the only feasible values that the original forward model can yield. Therefore, the only possible solution of the problem lays in the intersection between the curves given by expression (49) and (52) as shown in Figure 6c. Combining all the information, the *a posteriori* parameter probability function is a Dirac function which concentrate all the probability on the solution $m = 1.3 \cdot 10^5\,\mathrm{kN} \cdot \mathrm{m}^2$:

$$\sigma_m(m) = \delta(m - 1.3 \cdot 10^5) \tag{53}$$

Note that this example is a conventional minimization problem:

$$\min_m \left(d_{obs} - g\left(m\right)\right)^2 = \min_m \left(1.75 \cdot 10^{-3} - \frac{227.55}{m}\right)^2 \tag{54}$$

subjected to the restrictions:

$$10^5 \leq m \leq 3.5 \cdot 10^5 \tag{55}$$

5.1.3 Problem A resolution with surrogate forward model

In the case that the original forward model were computationally very demanding, the numerical burden could be minimized substituting the original forward model $g(m)$ (48) by a surrogated linear model $\tilde{g}(m)$:

$$g(m) \approx \tilde{g}(m) = a_0 + a_1 m \tag{56}$$

When the model model $g(m)$ is replaced by $\tilde{g}(m)$ a truncation error ε_t arises. Assuming that the truncation error is normally distributed, the predicted response of the surrogated model $\tilde{g}(m)$ is given by equation (57) as shown in Figure 7(b).

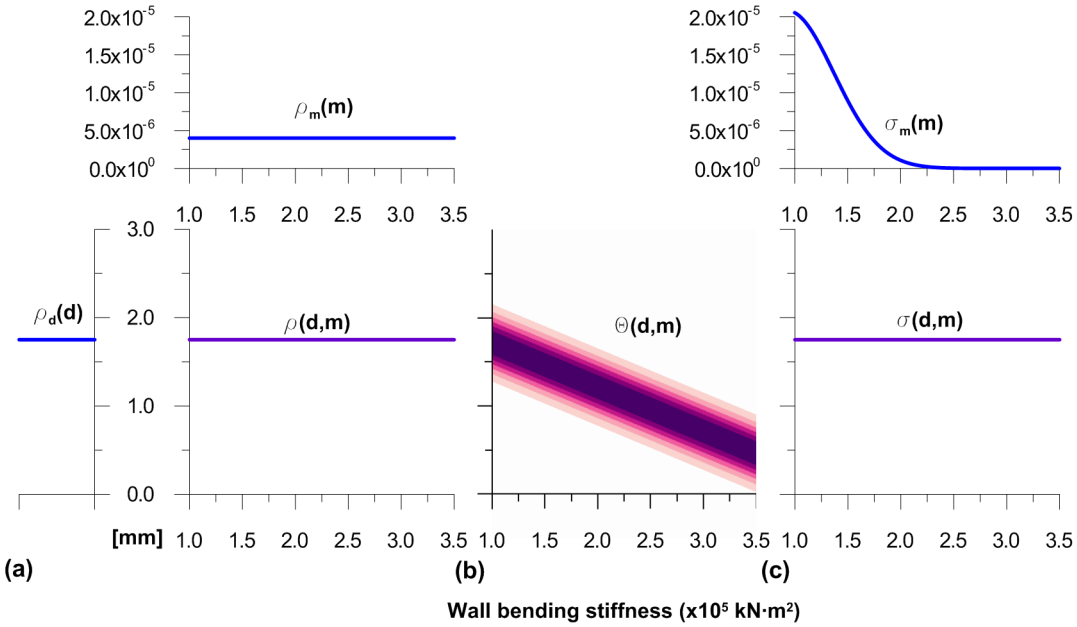

Figure 7: Bayesian resolution of problem A using a surrogate forward model. 1st Iteration. No observational uncertainties but modelling error due to surrogation (a) parameters and observations *a priori* pdf, (b) model pdf and (c) parameters and observations *a posteriori* pdf.

Table 2: Evolution of the parameter range and point of maximum likelihood when using a surrogate model to solve problem A.

Iteration	Initial Range	Final Range	PML
1st	$10^5 - 3.50 \cdot 10^5$	$10^5 - 1.82 \cdot 10^5$	10^5
2nd	$10^5 - 1.82 \cdot 10^5$	$1.20 \cdot 10^5 - 1.45 \cdot 10^5$	$1.32 \cdot 10^5$
3rd	$1.20 \cdot 10^5 - 1.45 \cdot 10^5$	$1.29 \cdot 10^5 - 1.31 \cdot 10^5$	$1.30 \cdot 10^5$
4th	$1.29 \cdot 10^5 - 1.31 \cdot 10^5$	$1.30 \cdot 10^5 - 1.30 \cdot 10^5$	$1.30 \cdot 10^5$

$$\Theta\left(d,m\right) = \begin{cases} \frac{1}{\sqrt{2\pi \cdot \mathrm{var}(\varepsilon_t)}} \exp\left(-\frac{1}{2}\frac{(d-\tilde{g}(m))^2}{\mathrm{var}(\varepsilon_t)}\right) & m \in \left[10^5, 3.5 \cdot 10^5\right] \\ 0 & m \notin \left[10^5, 3.5 \cdot 10^5\right] \end{cases} \tag{57}$$

Combining the *a priori* knowledge of the observation and the sought parameter (Figure 7a) with the information offered by the surrogate model (Figure 7b), the solution of the problem is a truncated Gauss distribution (Figure 7c). That solution is an improvement from the initial guess but it is still far away from the true solution because it incorporates the uncertainty introduced by the surrogate model. If the 95% confidence interval of that distribution is taken, after that first iteration $m \in \left[10^5, 1.82 \cdot 10^5\right]$ and the process is repeated again, the solution improves as depicted in Figure 8. The process is repeated iteratively four times to make converge the *a posteriori* parameter pdf to a Dirac pdf which concentrates all the probability of occurrence on the true solution as shown in Figures 7, 8, 9 and 10 and summarized in Table 2.

Figure 11 offers a graphical explanation of the process. The initial parameter range is too wide and a first

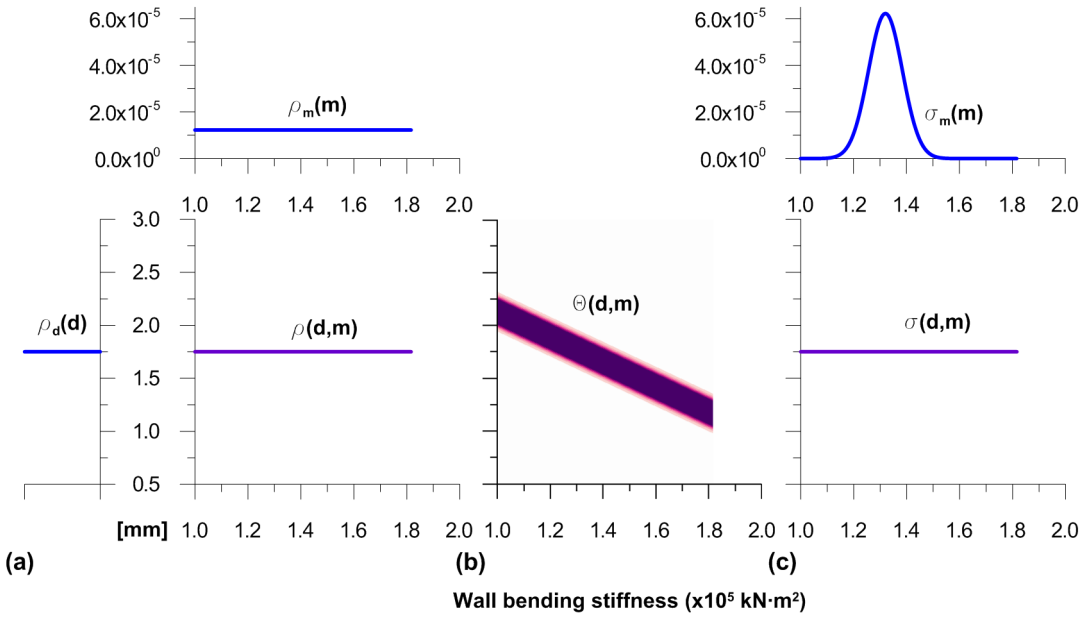

Figure 8: Bayesian resolution of problem A using a surrogate forward model. 2nd Iteration. No observational uncertainties but modelling error due to surrogation (a) parameters and observations *a priori* pdf, (b) model pdf and (c) parameters and observations *a posteriori* pdf.

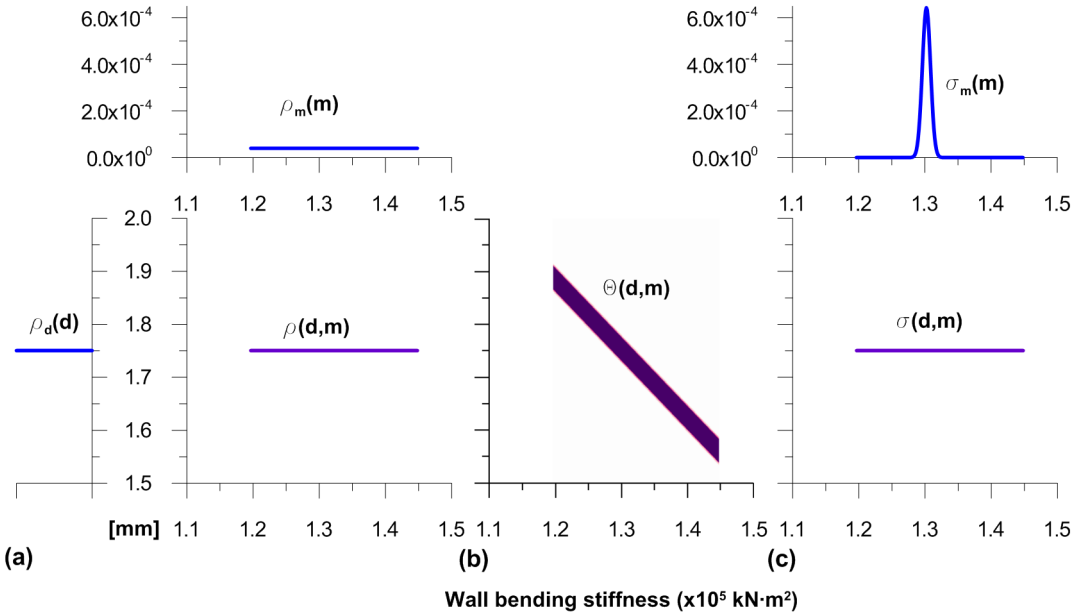

Figure 9: Bayesian resolution of problem A using a surrogate forward model. 3rd Iteration. No observational uncertainties but modelling error due to surrogation (a) parameters and observations *a priori* pdf, (b) model pdf and (c) parameters and observations *a posteriori* pdf.

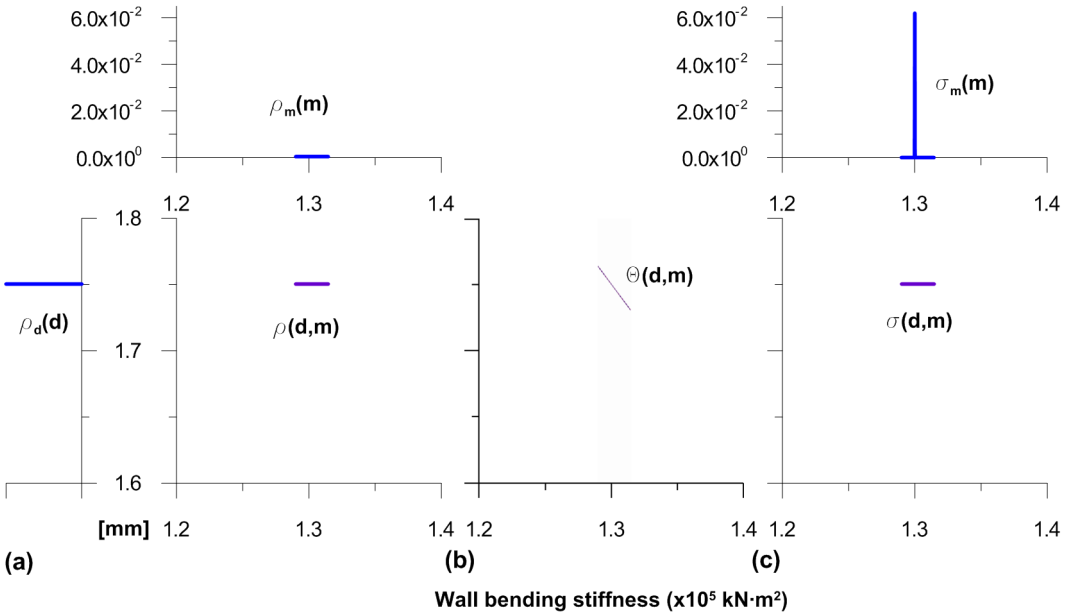

Figure 10: Bayesian resolution of problem A using a surrogate forward model. 4th Iteration. No observational uncertainties but modelling error due to surrogation (a) parameters and observations *a priori* pdf, (b) model pdf and (c) parameters and observations *a posteriori* pdf.

Table 3: Model parameters adopted to generate problem B observations d_{obs} (E Young modulus, ν Poisson's ratio, γ density, ϕ' friction angle, c' cohesion, K_0 at rest pressure coefficient, μ soil-wall friction coefficient)

Material	E (kPa)	ν	γ (kN/m^3)	ϕ'	c' (kPa)	K_0	μ
Sand	$2{\cdot}10^4$	0.30	20	32	0	0.47	0.35
Concrete	$1.8{\cdot}10^7$	0.20	25	-	-	-	-

degree polynomial surrogate model does not fit well to the original forward model curve. As the parameter range is narrowed to the higher probability intervals, the surrogate model approximates better and better to the original model.

5.2 Synthetic excavation (Problem B)

5.2.1 Problem B definition

The model presented in Figure 12 represents a 0.60 m thick cantilever concrete diaphragm wall cast 12.0 m into the ground to retain a 4.0 m excavation cut. The aim of this problem is to determine $N = 5$ model parameters from $n = 12$ wall horizontal displacement which might represent inclinometer readings from a diaphragm concrete wall after an excavation. The vector of observations $\mathbf{d}_{obs}$ is generated synthetically adopting the parameters in Table 3 to avoid modelling and observational errors. The observed displacements $\mathbf{d}_{obs}$ are presented in Table 4 and depicted in Figure 13.

The forward model used to simulate the excavation is the finite element model shown at Figure 12. The analysis is carried out in two stages: (i) the initial stress state is generated imposing a given at rest coefficient K_0 and

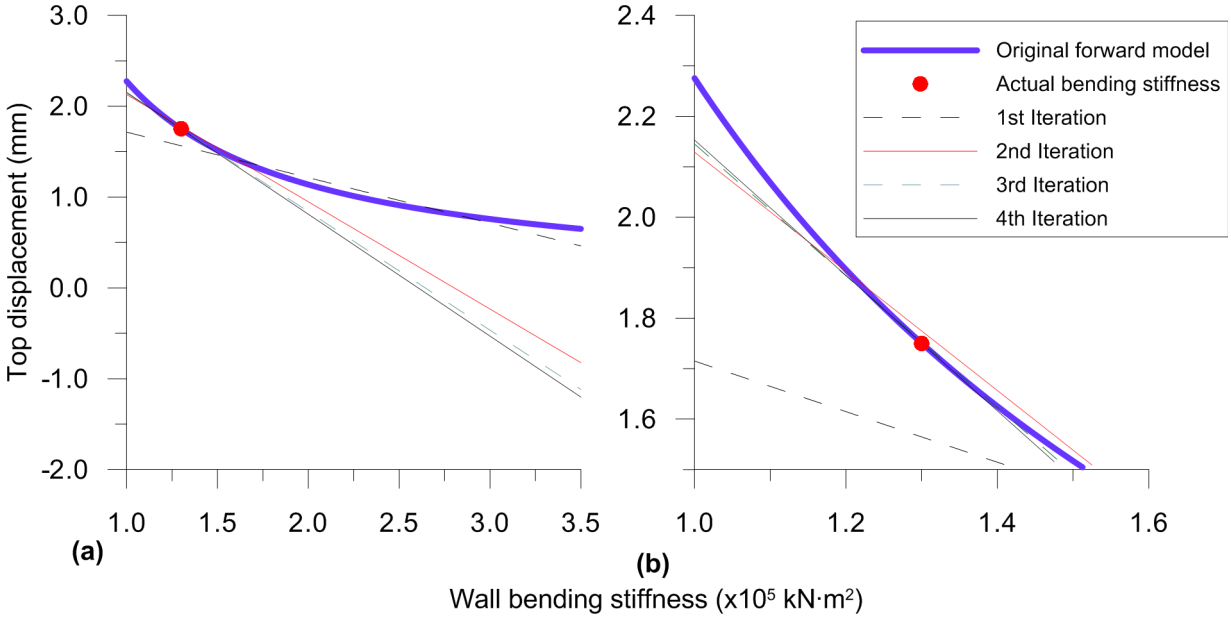

Figure 11: Graphical explanation of the iterative scheme in the resolution of problem A case using a surrogate model (a) general view (b) zoomed view.

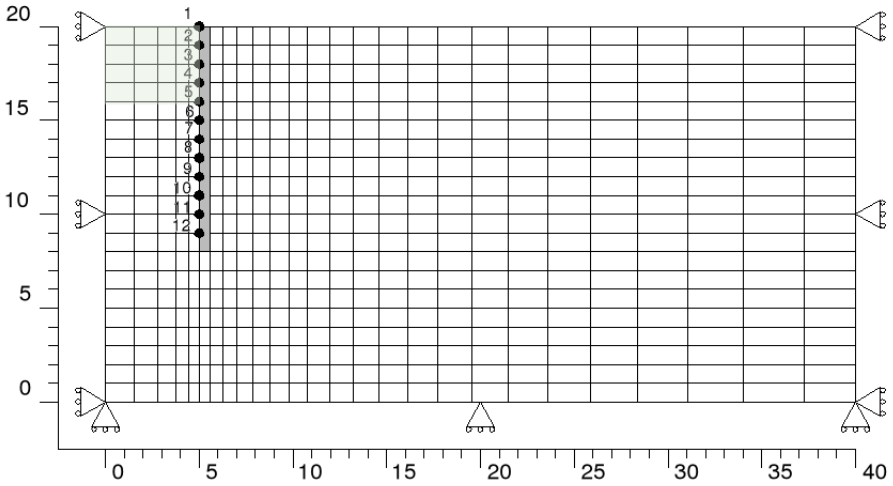

Figure 12: Synthetic excavation (Problem B). Plane strain ABAQUS CAE 6.11-1 FEM mesh and $n = 12$ observation points in the analysis. Dark grey elements represent the concrete wall and light grey elements are the excavated elements.Implicit integration. Soil (Mohr Coulomb material): 508 4 nodes quadrilateral elements (CPE4), wall (elastic material): 12 8 nodes quadrilateral elements (CPE8). Interaction between wall and soil simulated using penalty method ([36] for further details).

Table 4: Synthetic excavation (Problem B). Diaphragm wall horizontal displacements d_{obs} computed from parameters in Table 3

Point	Displacement (mm)	Point	Displacement (mm)
1	-10.9	7	-5.9
2	-10.0	8	-5.5
3	-9.0	9	-5.2
4	-8.1	10	-5.1
5	-7.2	11	-5.0
6	-6.4	12	-4.9

Table 5: Initial parameter range considered in problem B (Source $^{(*)}$ [37] $^{(**)}$ [38])

Parameter	Range
Concrete wall Young Modulus (E_c)	$1.5{\cdot}10^7 - 3.5{\cdot}10^7$ kPa
Sand Young Modulus (E_s)	$8{\cdot}10^3 - 3{\cdot}10^4$ kPa$^{(*)}$
Sand friction angle (ϕ')	$30 - 40\,^{\circ(*)}$
At rest pressure coefficient (K_0)	$0.35 - 1.00^{(*)}$
Wall-soil friction coefficient (μ)	$0.20 - 0.40^{(**)}$

(ii) after that, the whole excavation is simulated deactivating the correspondent elements. The ground is a thick alluvial deposit of medium cohesionless sand which is modelled as a Mohr-Coulomb material. The concrete wall behaves as an isotropic elastic material. No water level is considered.

5.2.2 Problem B resolution

The parameters to be identified from d_{obs} are the Young modulus of the soil and the concrete wall (E_s and E_c respectively), the soil angle of friction (ϕ'), the initial at rest coefficient (K_0) and the wall-soil friction coefficient (μ). The number observations is greater than the number of parameters. The uniform parameter joint pdf encoding the initial information in Table 5 is the straightforward choice:

$$\rho_m(\mathbf{m}) = \begin{cases} \dfrac{1}{2 \cdot 10^7 \cdot 22000 \cdot 10 \cdot 0.65 \cdot 0.2} & \begin{array}{l} E_c \in \left[1.5 \cdot 10^7, 3.5 \cdot 10^7\right], \\ E_s \in [8000, 30000], \\ \varphi \in [30, 40], \\ K_0 \in [0.35, 1], \\ \mu \in [0.2, 0.4] \end{array} \\ 0 & \text{for any other value} \end{cases} \tag{58}$$

In this case, the parameter support of each parameter m_i is normalized to $\xi_i \in [\ -1 \quad 1\ ]$ using the following transformation:

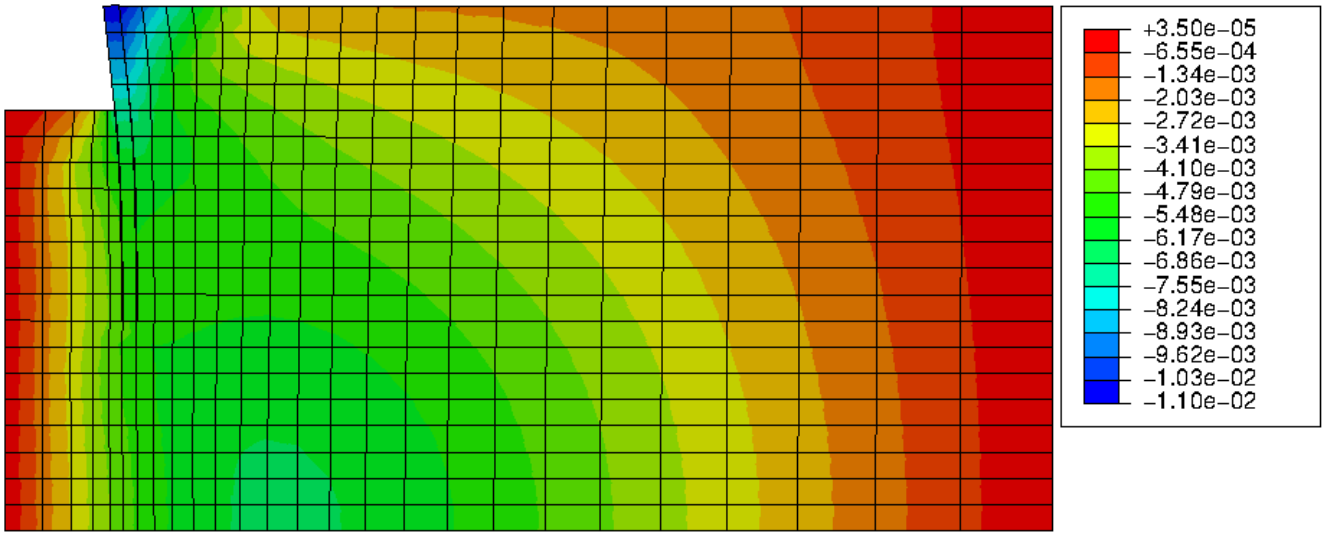

Figure 13: Horizontal displacement obtained from the model (Problem B)

$$\xi_i = -1 + 2\frac{m_i - m_{i\,\min}}{m_{i\,\max} - m_{i\,\min}} \tag{59}$$

The prior pdf (58) becomes:

$$\rho_\xi(\boldsymbol{\xi}) = \begin{cases} 1/2^5 & \xi_i \in [-1,1] \\ 0 & \xi_i \notin [-1,1] \end{cases} \tag{60}$$

In this problem, there is no observational error. For that reason the *a priori* joint parameter and observation pdf is:

$$\rho(\boldsymbol{\xi}, \mathbf{d}) = \begin{cases} 1/2^5 & \xi_i \in [-1,1] \quad \text{and} \quad \mathbf{d} = \mathbf{d}_{obs} \\ 0 & \xi_i \notin [-1,1] \quad \text{or} \quad \mathbf{d} \neq \mathbf{d}_{obs} \end{cases} \tag{61}$$

The numerical burden is minimized using a linear model for each observation as shown in expression (16). As the *a priori* probability distribution functions are expressed in terms of uniform distributions, the expansion coefficients u_{ij} in equation (16) are computed from combinations of the Legendre polynomial roots (see Table 1) using the strategy presented by Sudret [29].

The solution must incorporate the truncation error resulting from replacing $\mathbf{g}(\mathbf{m})$ by $\tilde{\mathbf{s}}(\boldsymbol{\xi})$ and quantified using the covariance matrix $\mathbf{C}_T$ whose determination is described in previous sections:

$$\sigma_{\boldsymbol{\xi}}(\boldsymbol{\xi}) \propto \begin{cases} \exp\left(-\frac{1}{2}[\mathbf{d}_{obs} - \tilde{\mathbf{s}}(\boldsymbol{\xi})]^T \mathbf{C}_T^{-1} [\mathbf{d}_{obs} - \tilde{\mathbf{s}}(\boldsymbol{\xi})]\right) & \xi_i \in [-1,1] \\ 0 & \xi_i \notin [-1,1] \end{cases} \tag{62}$$

As the diaphragm wall is a very stiff structure, the displacements of nearby points are highly correlated, thus the truncation errors. For that reason, matrix $\mathbf{C}_T$ is a 12×12 ill conditioned matrix. As the only source of uncertainty are the $N = 5$ model parameters, covariance matrix $\mathbf{C}_T$ is approximated using its five higher eigenvalues as equation (22) indicates. Hence expression (62) becomes:

$$\sigma_{\boldsymbol{\xi}}(\boldsymbol{\xi}) \propto \begin{cases} \exp\left(-\frac{1}{2}\left[(\mathbf{d}_{obs} - \tilde{\mathbf{s}}(\boldsymbol{\xi}))^T \tilde{\mathbf{V}}\right] \tilde{\mathbf{D}}^{-1} \left[(\mathbf{d}_{obs} - \tilde{\mathbf{s}}(\boldsymbol{\xi}))^T \tilde{\mathbf{V}}\right]^T\right) & \xi_i \in [-1,1] \\ 0 & \xi_i \notin [-1,1] \end{cases} \tag{63}$$

The probability distribution function of the parameters is obtained marginalizing the *a posteriori* pdf (63). As the exponent of that equation is a quadratic expression, the numerical integration is relatively light. The first row of Figure 14 presents the solution obtained from the surrogated model $\tilde{\mathbf{s}}(\boldsymbol{\xi})$ built with Table 5 ranges. Since the surrogate model is a poor approximation of the original forward model, the variance of the solution is ample. Limiting the ranges to the 95% confidence interval and repeating the process with those ranges, the solution of the problem improves (second row of Figure 14). After six iterations the *a posteriori* marginal probability distribution functions converge to a Dirac pdf which concentrate all the occurrence probability in the true parameter set. Figure 14 depicts the whole iterative process.

The most likely model parameters are obtained minimizing the exponent of expression (63) as described previously. Figure 15 shows the evolution of the parameter maximum likelihood values as the iterations progresses together with the 95% confidence interval which narrows quickly. The truncation error, measured by the trace of $\mathbf{C}_T$, decreases in a exponential way as shown in Figure 16. Figure 17 depicts the predictions of the diaphragm wall movements together with the 95% confidence prediction interval in the iterative process. The prediction is very good even at the first iteration. One of the advantage of the proposed methodology is that a statistical measure of goodness-of-fit at every iteration is available.

The computational cost of solving this problem comes from running the original forward model. It has been necessary 24 runs to built the surrogate model (see [29] for details) and 80 runs to compute the truncation error. As six iterations have been required to reach to the solution, a total amount of 624 executions of the forward model have been needed ($6 \times 24 + 6 \times 80$). Every original forward model run took in average 20 seconds to complete. Hence the overall optimization process took around 4 hours.

5.3 Hochstetten Excavation (Problem C)

5.3.1 Hochstetten Excavation problem definition

The aim of this problem is to calibrate $N = 9$ soil parameters from the $n = 14$ horizontal wall inclinometer measures (see Table 6) in a 4 m wide strutted excavation. The excavation depth was 5 m and it was achieved in six stages. In the seventh stage, a 1 m high basin was filled with water to impose a surcharge on the ground

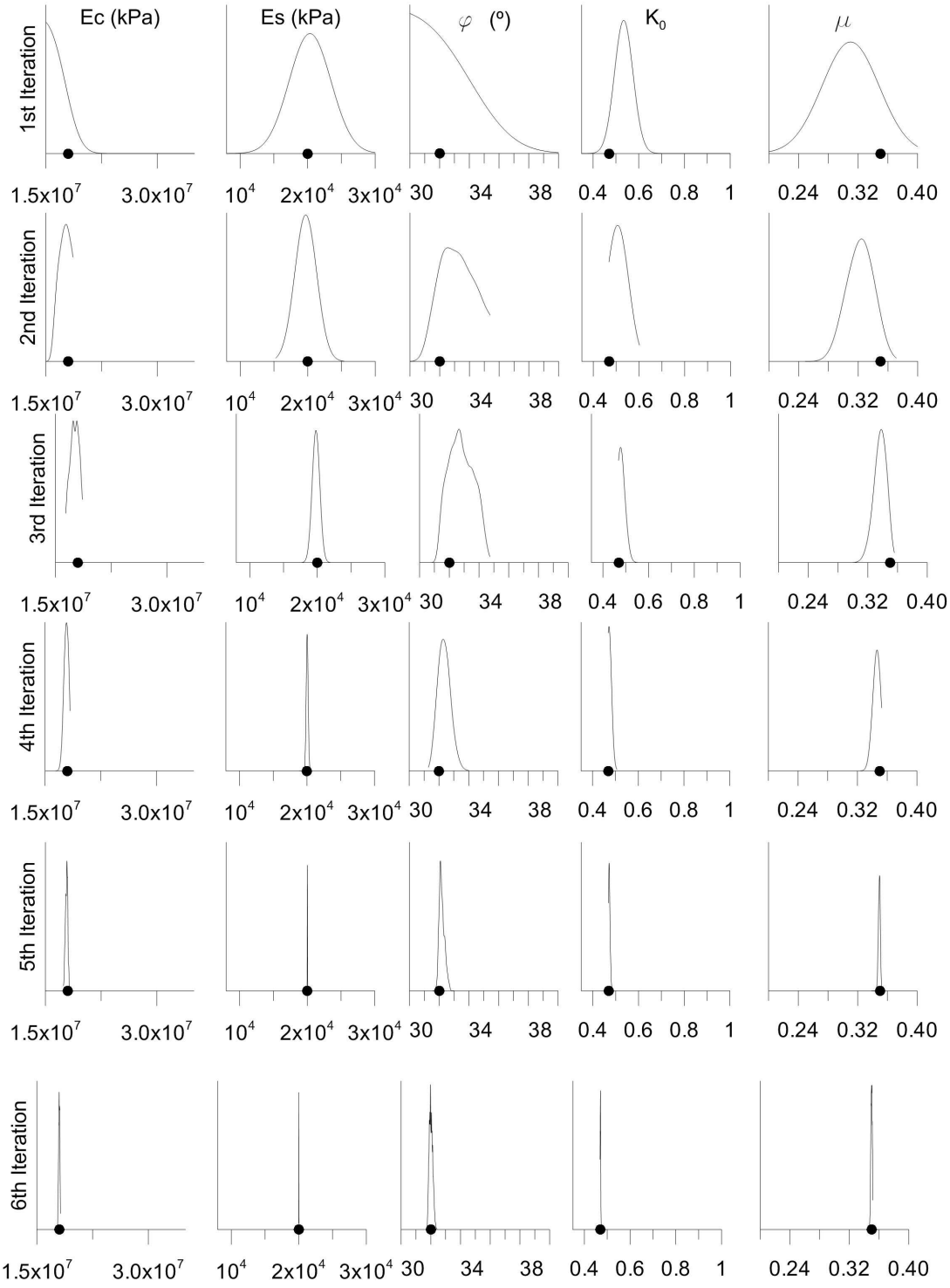

Figure 14: Problem B parameter marginal probability distribution function evolution. The point on the graphs indicates the parameter true value.

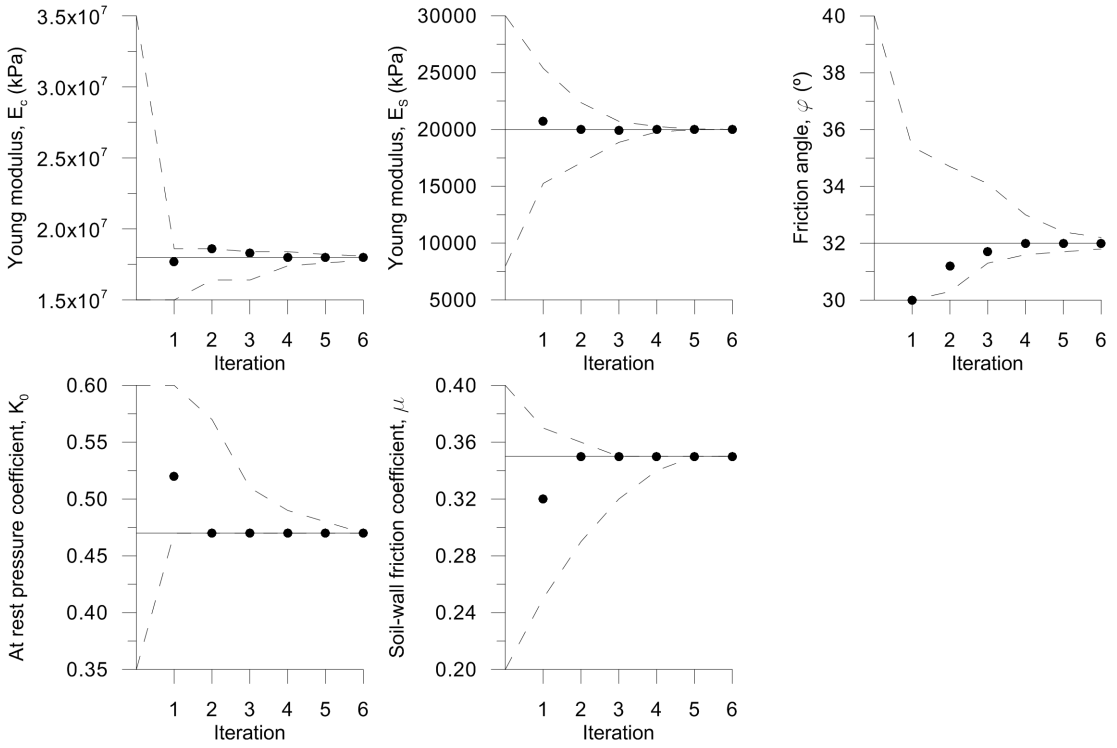

Figure 15: Problem B most likely parameter values (points) together with the 95% confidence interval (dotted line) per iteration

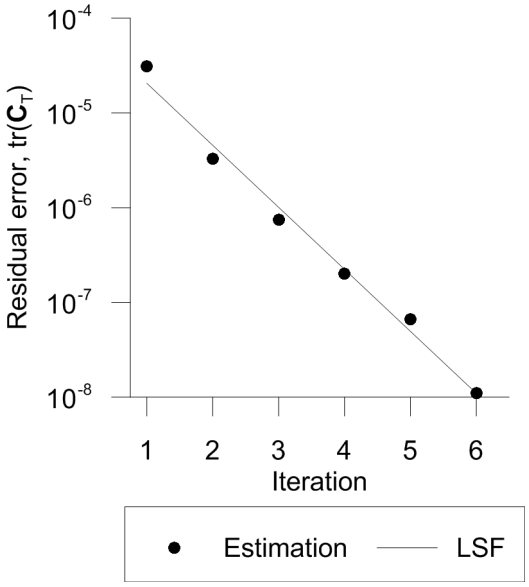

Figure 16: Problem B evolution of residual error $\mathrm{tr}(\mathrm{C_T})$ during the iterative process and least square fit

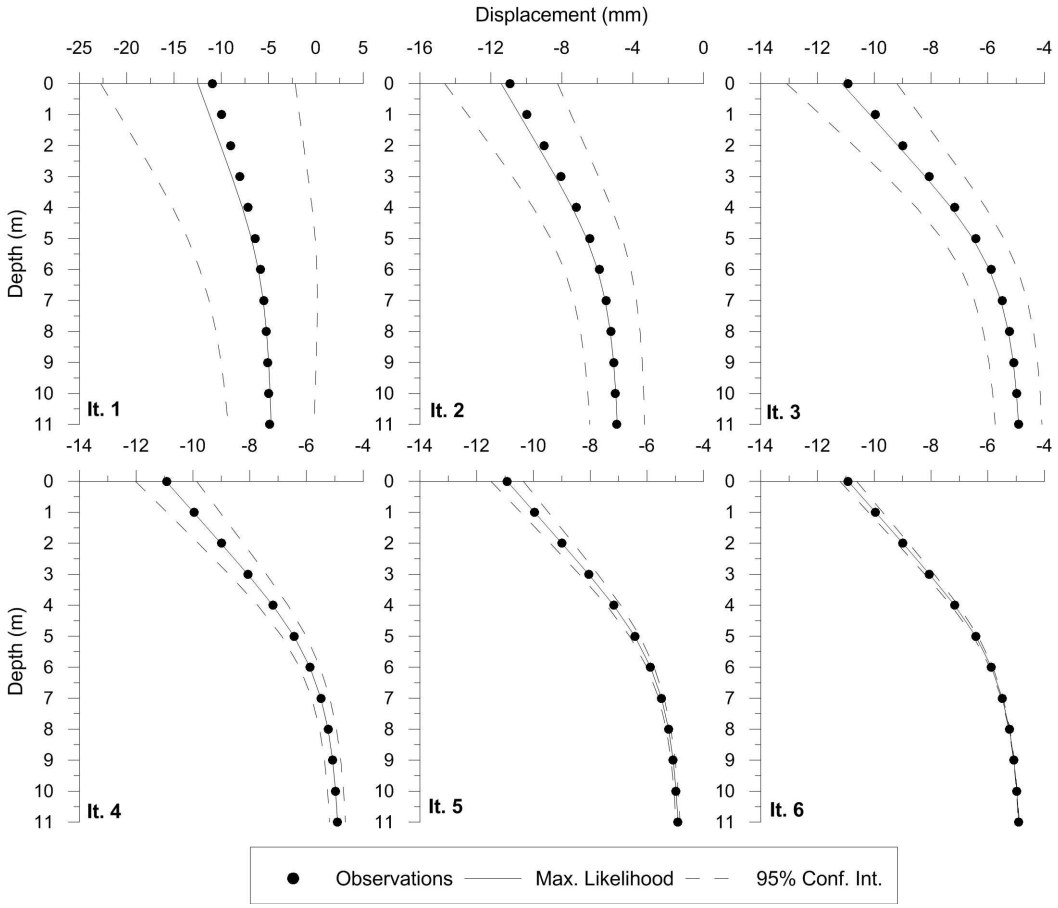

Figure 17: Problem B Prediction (continuous lines) at each iteration of the observed movements (point) together with the 95% confidence interval (dotted line)

Table 6: Hochstetten excavation (Problem C). Diaphragm wall horizontal displacements d_{obs} [33]. The initial stage is set when the excavation is up to 1.75 m depth and the struts are placed [35].

Point	Displacement (mm)	Point	Displacement (mm)
1	2.14	8	-3.26
2	1.97	9	-3.15
3	1.23	10	-2.43
4	0.31	11	-1.57
5	-0.72	12	-0.69
6	-2.04	13	0.00
7	-3.07	14	0.00

Table 7: Elastic parameters adopted for the sheet wall and strut in Hochstetten excavation (Problem C) (EA axial stiffness, EI bending stiffness, ν Poisson's ratio, w weight) [34]

Member	EA (kN/m)	EI (kNm^2/m)	ν	w
Sheet wall	$2.2{\cdot}10^6$	$2.0{\cdot}10^3$	0.3	0
Strut	$4.2{\cdot}10^6$	-	-	0

surface (see [33] for further details). Table 6 observations were taken when the water surcharge was applied.

The sheet walls were driven into a sandy deposit. The structural members (strut and sheet wall) have been regarded elastic materials (see Table 7). The soil has been divided into two layers: (i) the unsaturated upper layer which is above water table (5.5 m deep) and (ii) the saturated layer below the water table [34, 35]. Both soil levels have been simulated by means of an elasto-plastic Mohr-Coulomb model. The finite element model used as a forward model is described in Figure 18.

5.3.2 Hochstetten Excavation problem resolution

Table 8 presents the $N = 9$ parameters $\mathbf{m}$ to determine. The sandy levels only differ in the Young Modulus and cohesion. Table 8 also contains the adopted ranges defined from different sources [34, 35, 39]. After the normalization of $\mathbf{m}$ to $\boldsymbol{\xi}$ using the transformation in expression (59), the following *a priori* parameter pdf is considered:

$$\rho_\xi(\boldsymbol{\xi}) = \begin{cases} 1/2^9 & \xi_i \in [-1,1] \\ 0 & \xi_i \notin [-1,1] \end{cases} \tag{64}$$

Unlike the previous cases, this is a real problem and the precision of the observations and the accuracy of the model must be quantified. The sheet wall movements were measured with an inclinometer which precision might be affected by many factors [40]. Gens [41] after reviewing published analyses highlights that the lateral wall movements are not very sensitive to the type of constitutive model adopted, specially in stiff excavations. For

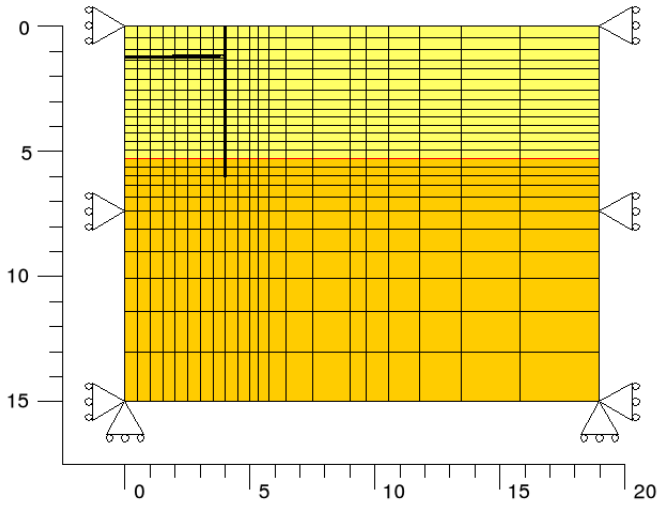

Figure 18: Hochstetten Excavation (Problem C). Plane strain ABAQUS CAE 6.11-1 FEM mesh. Implicit integration. Soil (Mohr Coulomb material): 525 4 nodes quadrilateral elements (CPE4), sheetwall (elastic material): 12 beam elements (B22), strut (elastic material) 8 truss elements (T2D2). Interaction between wall and soil simulated using penalty method ([36] for further details).

Table 8: Hochstetten excavation (Problem C). Initial parameter range

Parameter	Range
Unsaturated upper sand layer Young Modulus (E_1)	$10^4 - 4{\cdot}10^4\,\mathrm{kPa}$
Saturated sand layer Young Modulus (E_2)	$2 \cdot 10^4 - 5{\cdot}10^4\,\mathrm{kPa}$
Poisson's ratio (both layers) (ν)	$0.15 - 0.40$
At rest pressure coefficient (both layers) (K_0)	$0.20 - 0.60$
Sand friction angle (both layers) (φ)	$30 - 45\,^\circ$
Sand dilatancy angle (both layers) (ψ)	$5 - 20\,^\circ$
Unsaturated upper sand layer cohesion (c_1)	$0.3 - 10\,\mathrm{kPa}$
Saturated sand layer cohesion (c_2)	$0.3 - 10\,\mathrm{kPa}$
Wall-soil friction coefficient (μ)	$0.20 - 1.50$

those reasons, it is assumed that the differences between the predictions and the inclinometer readings are due to observational errors. In other words, the covariance matrix that encodes the epistemic error is $\mathbf{C}_G = \mathbf{0}$. As all the readings were taken with the same device, the observation errors are assumed independent and Gaussian with zero mean and σ_D^2 variance. It is considered that the 95% confidence interval of each displacement is ± 1 mm. That value approximately represents a standard deviation of 0.5 mm which represents a variance of $\sigma_D^2 = 2.5 \cdot 10^{-7}\,\mathrm{m}^2$. Hence, the covariance matrix $\mathbf{C}_D$ is a diagonal matrix $\mathbf{C}_D = \sigma_D^2 \mathbf{I}$ and the observations pdf using equation (3) is:

$$\rho_d\left(\mathbf{d}\right) = \frac{1}{\left(\sqrt{2\pi}/\sigma_D\right)^n} \cdot \exp\left[-\frac{1}{2}(\mathbf{d}-\mathbf{d}_{obs})^T \left[\frac{1}{\sigma_D^2}\mathbf{I}\right](\mathbf{d}-\mathbf{d}_{obs})\right] \tag{65}$$

Combining equations (64) and (65), the *a priori* parameter and observation joint distribution is:

$$\rho\left(\boldsymbol{\xi},\mathbf{d}\right) \propto \begin{cases} \exp\left[-\frac{1}{2}(\mathbf{d}-\mathbf{d}_{obs})^T \left[\frac{1}{\sigma_D^2}\mathbf{I}\right](\mathbf{d}-\mathbf{d}_{obs})\right] & \xi_i \in [-1,1] \\ 0 & \xi_i \notin [-1,1] \end{cases} \tag{66}$$

As in the previous cases, the FEM forward model is surrogated using a linear model $\tilde{\mathbf{s}}\left(\boldsymbol{\xi}\right)$ as seen in expression (16). Hence, a modelling error quantified in the covariance matrix $\mathbf{C}_T$ turns up. Once computed $\mathbf{C}_T$ as shown previously, the solution of the problem is obtained using equation (18):

$$\sigma_{\boldsymbol{\xi}}\left(\boldsymbol{\xi}\right) \propto \begin{cases} \exp\left[-\frac{1}{2}(\mathbf{d}_{obs}-\tilde{\mathbf{s}}\left(\boldsymbol{\xi}\right))^T \left(\sigma_D^2\mathbf{I}+\mathbf{C}_T\right)^{-1}(\mathbf{d}_{obs}-\tilde{\mathbf{s}}\left(\boldsymbol{\xi}\right))\right] & \xi_i \in [-1,1] \\ 0 & \xi_i \notin [-1,1] \end{cases} \tag{67}$$

The solution $\sigma_{\boldsymbol{\xi}}\left(\boldsymbol{\xi}\right)$ using $\tilde{\mathbf{s}}\left(\boldsymbol{\xi}\right)$ is initially a poor approximation. To improve the solution, a new iteration is performed using as *a priori* ranges the parameter 95% confidence intervals from the *a posteriori* parameter marginal pdf. Those distributions are obtained integrating equation (67). Due to that reduction of the search space, the agreement between the surrogate and the original model improves. That process is repeated until the truncation error is an order the magnitude less than the observation error. Fifteen iterations have been required to achieve a good fit between the original and the surrogate model. Figure 19 shows that the most likely parameters are able to reproduce properly the sheet wall movements even at the initial iterations. The statistical information gathered during the calibration process enables to display in Figure 19 the 95% confidence prediction intervals which is an indication of the fit goodness.

As in the previous case, the computational cost of solving this problem comes from computing the original forward model. It has been necessary 80 runs to build the surrogate model and 144 runs to compute the truncation error. The reduction of the truncation error is exponential as shown in Figure 20. Furthermore, the plot iteration number versus log-error depicted in Figure 20 suggested a linear pattern. A line was fitted to the log-data from the nine first iteration to estimate the truncation error. For that reason, the computational burden have been alleviated in the six last iterations. Hence, a total amount of 2496 executions $(9 \times (80 + 144) + 6 \times 80)$ of the

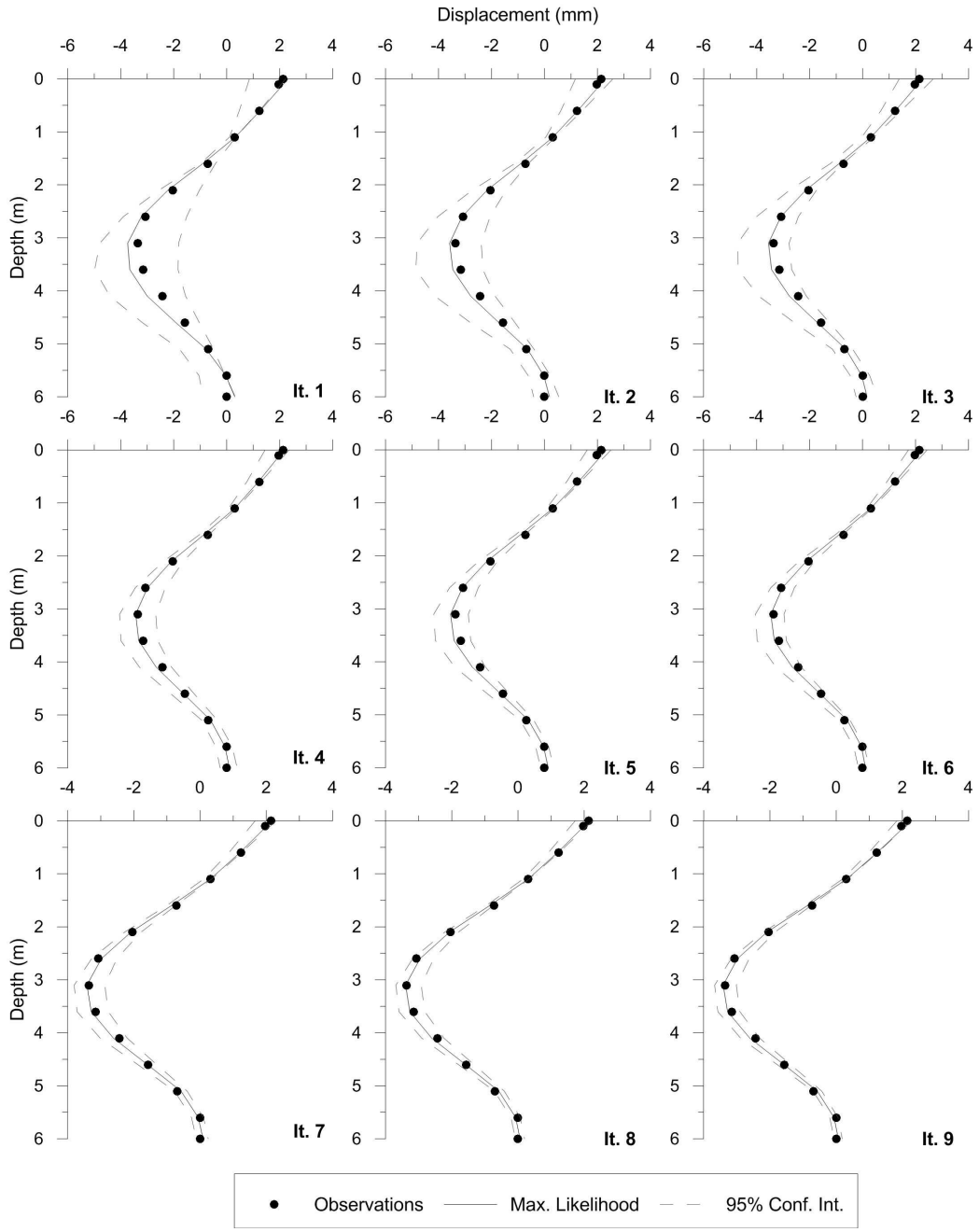

Figure 19: Problem C wall displacement prediction (from 1st to 9th iteration) with most likely values and 95% confidence parameters

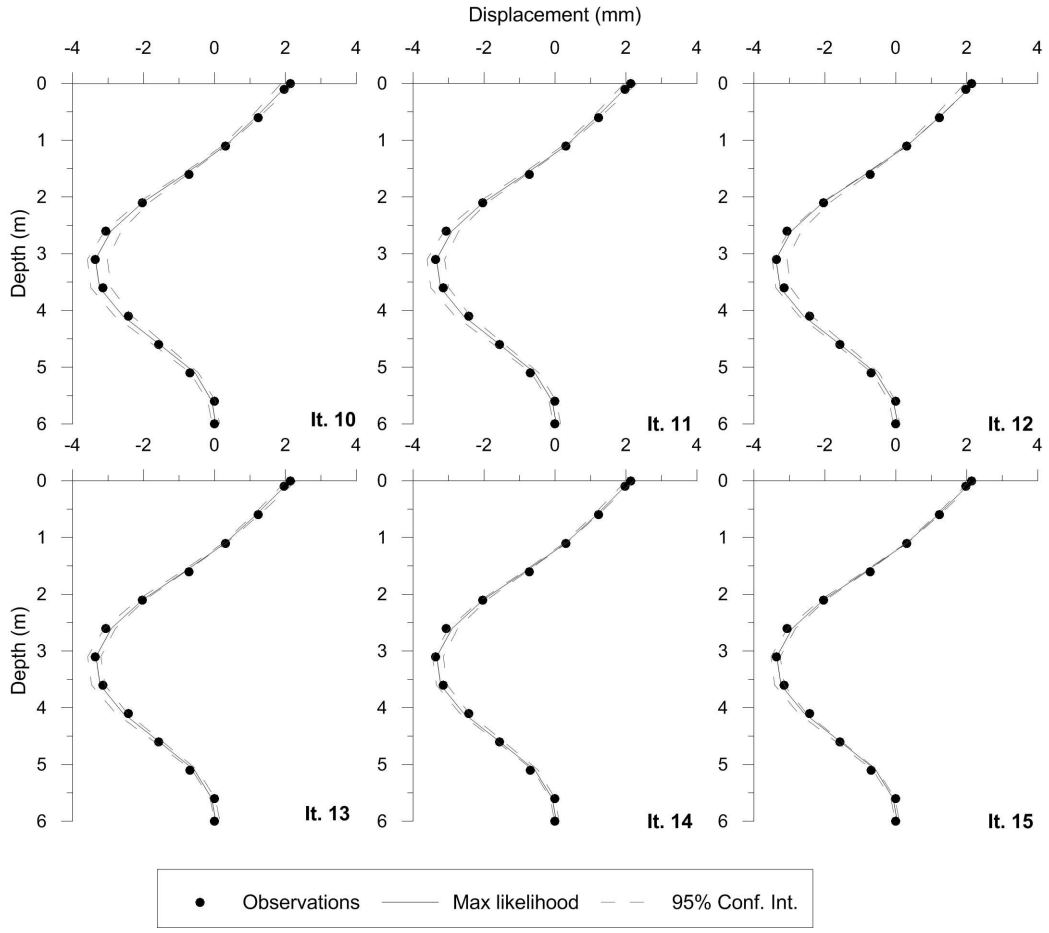

Figure 19: (continued) Problem C wall displacement prediction (from 10th to 15th iteration) with most likely values and 95% confidence parameters

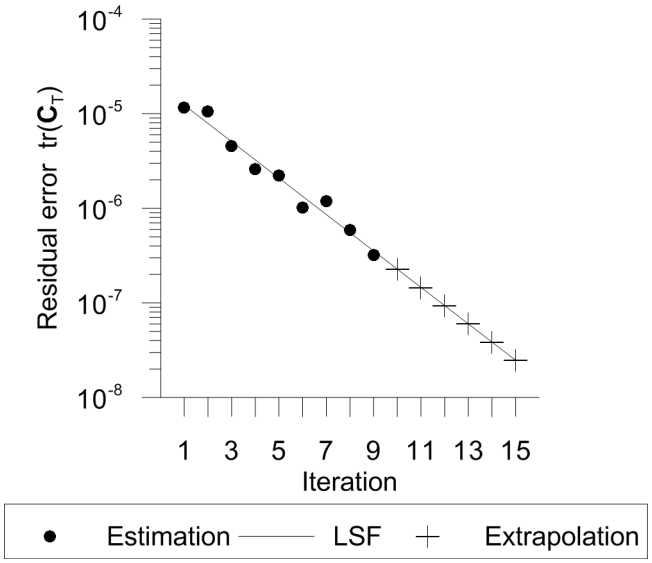

Figure 20: Problem C residual error estimation. Dots indicate residual error computed with the proposed methodology and crosses are linear fit extrapolations

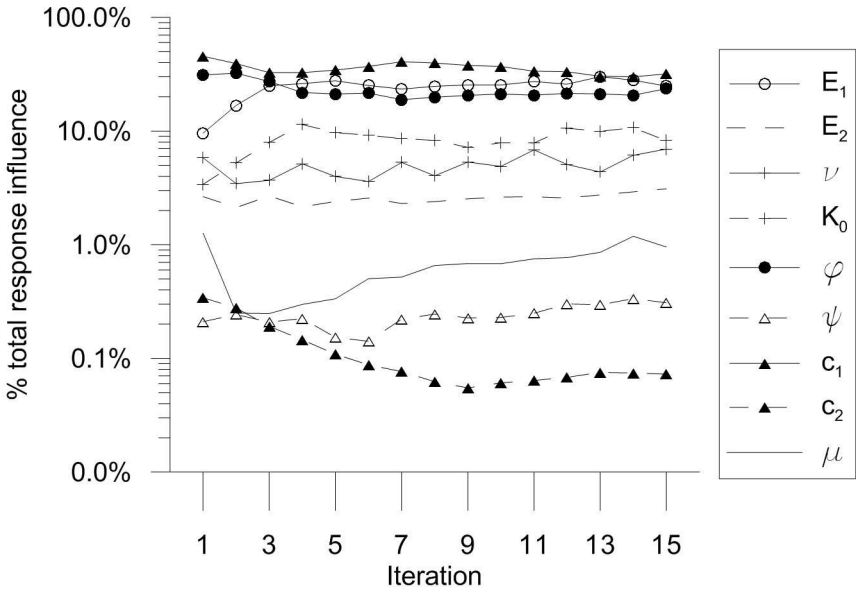

Figure 21: Problem C Parameter influence in the overall response variance

forward model have been needed. Every original forward model run took in average 35 seconds to complete. Hence the overall optimization process took around 25 hours.

The proposed methodology enables to disaggregate the overall variance by individual parameter as depicted in Figure 21. This result shows which parameters have more influence in the response variance. In this case, the upper unsaturated layer Young modulus E_1 and cohesion c_1 together with the friction angle φ represent more than the 80% of the total variance. The saturated layer Young modulus E_2, the Poison's ratio ν and the at rest pressure coefficient K_0 mean the 19% of the overall variance. The saturated layer cohesion c_2, the dilatancy angle ψ and the soil-wall friction μ hardly amount a 1% of the response. In the light of those results, the latter parameters could have been fixed to a certain value and the analysis could have been performed with six parameter instead of nine. As a result of that model reduction, the numerical burden to construct the surrogate model and to evaluate the surrogation error would have dropped to 35 and 96 realizations respectively. Therefore, a total of 1668 realizations $(3 \times (80 + 144) + 6 \times (35 + 96) + 6 \times 35)$ of the original forward model would have been required, a third less than considering all the parameters throughout the whole calibration process.

The evolution of the parameter marginal probability distribution functions is depicted in Figure 22. As the residuals are assumed Gaussian, those pdf are truncated Gaussian. The bell shape is very well defined in the variance greater weight parameters whereas an almost flat line is observed in the less important parameters.

Figure 23 depicts the evolution of the most likely parameter values which tends to stabilize as the iteration process progresses. That figure also shows the 95% confidence intervals which narrows quickly in line with the variance exponential reduction represented in Figure 20.

Table 9 summarizes the analysis results indicating the most likely parameters, the 95% confidence interval and the influence in the response of each parameter. A remarkable reduction in the parameter range has been achieved.

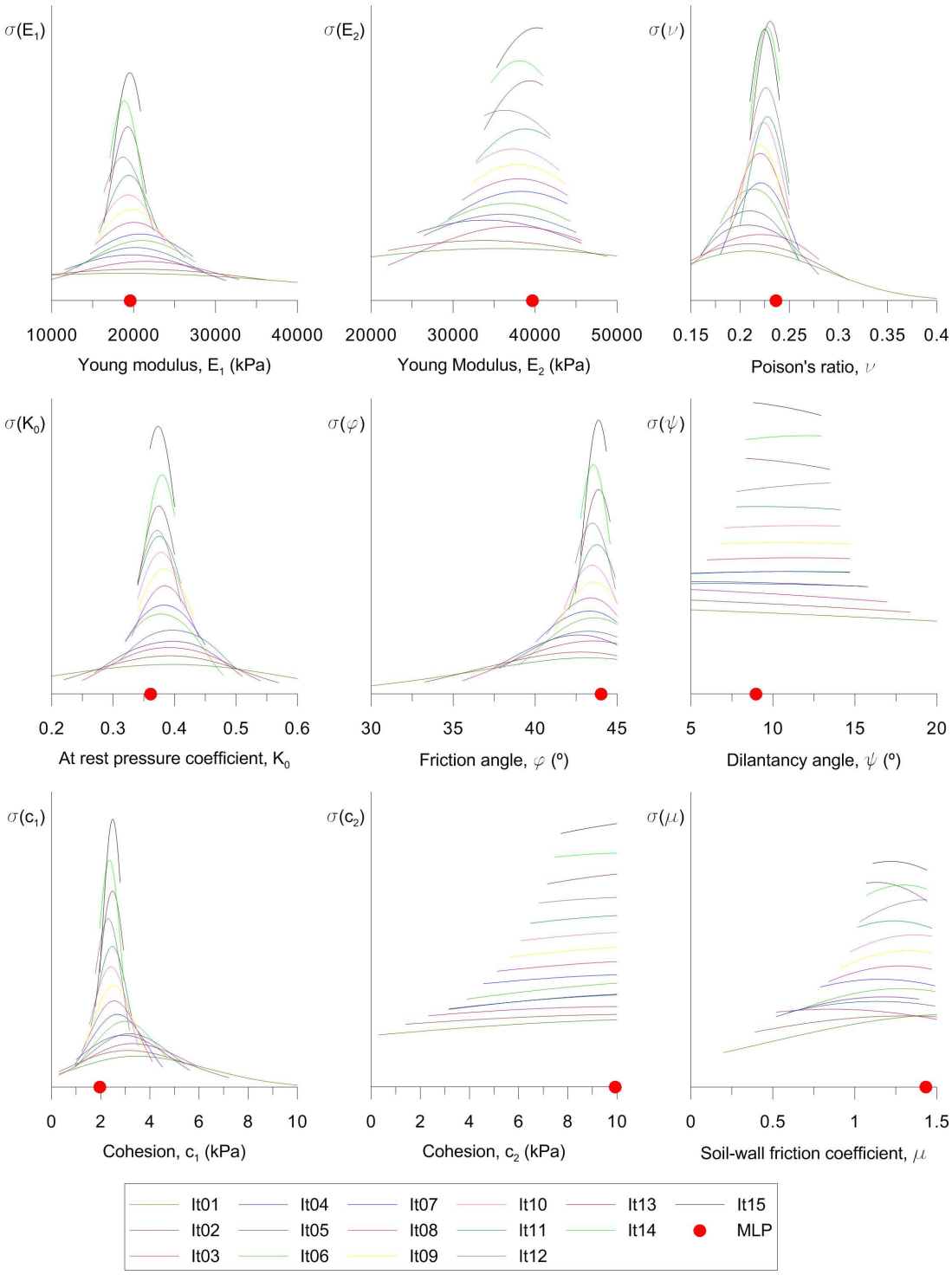

Figure 22: Problem C. Evolution of marginal probability density functions (lines, vertical axis not scaled) and most likely parameter (solid dot)

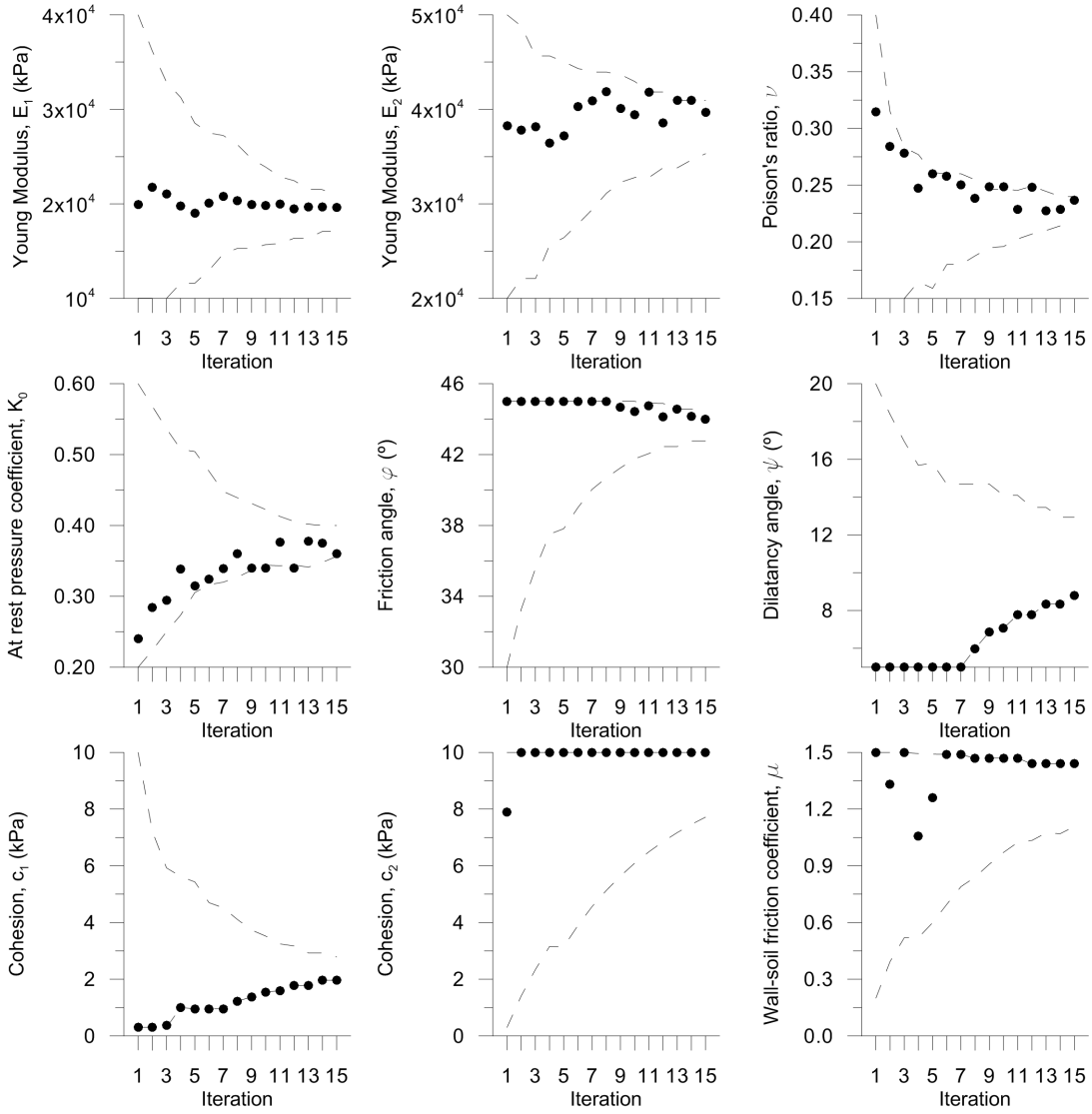

Figure 23: Problem C. Evolution of most likely parameter values and 95% confidence interval

Table 9: Hochstetten excavation (Problem C). Inverse problem solution: most likely parameter, 95% confidence interval and parameter variance influence.

Parameter	M.L.	Final range	Influence
Unsaturated upper sand layer Young Modulus (E_1)	19640 kPa	17095 – 20850 kPa	24.9%
Saturated sand layer Young Modulus (E_2)	39705 kPa	35315 – 40970 kPa	3.1%
Poisson's ratio (both layers) (ν)	0.24	$0,21 - 0.24$	7.0%
At rest pressure coefficient (both layers) (K_0)	0.36	$0.36 - 0.40$	8.2%
Sand friction angle (both layers) (φ)	44.0°	$42.8 - 44.3\,^\circ$	23.6%
Sand dilatancy angle (both layers) (ψ)	8.88.8°	$8.8 - 12.9\,^\circ$	0.3%
Unsaturated upper sand layer cohesion (c_1)	2.0 kPa	2.0 – 2.8 kPa	31.9%
Saturated sand layer cohesion (c_2)	10.0 kPa	7.7 – 10.0 kPa	0.1%
Wall-soil friction coefficient (μ)	1.4	1.10 – 1.40	1.0%

6 Conclusions

An innovative method to solve deep excavation inverse problems which takes advantage of Bayesian inference and the non-intrusive stochastic finite elements has been presented. The Bayesian inference is the most consistent way to tackle the inverse problem resolution because the yielded solution includes the uncertainty in the model and observations. The non intrusive SFEM based on the stochastic spectral methods can be seamlessly integrated in the Bayesian methodology and it is advantageous in two levels: (i) lightening heavy numerical burden of the deep excavation geotechnical models and (ii) disclosing statistical structure which improves the problem understanding.

The proposed methodology makes use of the non-intrusive SFEM to replace the numerical heavy original forward model by a lighter surrogate model built out of a polynomial chaos expansion (PCE). The main drawback of surrogating the forward model is that a modelling error arises because the surrogate fails to perfectly represent the original model. In this paper, a new technique which does not increases substantially the numerical burden to bound the surrogation error has been developed. That technique enables to tackle an iterative strategy to rapidly converge to the inverse problem solution. Furthermore, the spectral representation of the forward model makes possible to obtain a closed form of the covariance matrix between observations and it also enables to obtain the influence per parameter in the overall response.

The proposed methodology has been successfully tested in three problems of increasing difficulty. The results yielded by those analysis have proved very useful because provides greater insight to the technician carrying out the model calibration and set sound foundations for a model reduction.

References

[1] Kempfert, H.G., Gebreselassie, B.. Excavations and foundations in soft soils. Berlin: Springer-Verlag; 2006. ISBN 3540328947 (hd.bd.). URL http://dx.doi.org/10.1007/3-540-32895-5.

[2] Ou, C.Y.. Deep excavation: Theory and practice. London: Taylor & Francis; 2006. ISBN 0415403308.

[3] Co-operation in Science and Technology (COST) Action C7, . Guidelines for the Use of Advanced Numerical Analysis. London: Thomas Telford; 2002. URL http://www.icevirtuallibrary.com/content/book/100455.

[4] Kulhawy, F.H., Phoon, K.K.. Observations on geotechnical reliability-based design development in North America. In: Honjo, Y., Kusakabe, O., Matsui, K., Pokharel, G., editors. Proceedings International Workshop on Foundation Design Codes and Soil Investigation in view of International Harmonization and Performance Based Design. Tokyo: Balkema; 2002, p. 31–48.

[5] Puzrin, A.M., Alonso, E.E., Pinyol, N.M.. Geomechanics of failures. Dordrecht: Springer; 2010. ISBN 9048135311.

[6] Calvello, M., Finno, R.J.. Selecting parameters to optimize in model calibration by inverse analysis. Computers and Geotechnics 2004;31(5):411–425. doi:10.1016/j.compgeo.2004.03.004. URL http://dx.doi.org/10.1016/j.compgeo.2004.03.004.

[7] Chua, C.G., Goh, A.T.C.. Estimating wall deflections in deep excavations using Bayesian neural networks. Tunnelling and Underground Space Technology 2005;20(4):400–409. URL http://dx.doi.org/10.1016/j.tust.2005.02.001.

[8] Finno, R.J., Calvello, M.. Supported excavations: Observational method and inverse modeling. Journal of Geotechnical and Geoenvironmental Engineering 2005;131(7):826–836. doi:10.1061/(ASCE)1090-0241(2005)131:7(826). URL http://dx.doi.org/10.1061/(ASCE)1090-0241(2005)131:7(826).

[9] Hashash, Y.M.A., Levasseur, S., Osouli, A., Finno, R.J., Malécot, Y.. Comparison of two inverse analysis techniques for learning deep excavation response. Computers and Geotechnics 2010;37(3):323–333. URL http://dx.doi.org/10.1016/j.compgeo.2009.11.005.

[10] Hsiao, E., Schuster, M., Juang, C.H., Kung, G.T.C.. Reliability Analysis and Updating of Excavation-Induced Ground Settlement for Building Serviceability Assessment. Journal of Geotechnical and Geoenvironmental Engineering 2008;134(10):1448–1458. doi:doi:10.1061/(ASCE)1090-0241(2008)134:10(1448). URL http://ascelibrary.org/doi/abs/10.1061/(ASCE)1090-0241(2008)134:10(1448).

[11] Rechea, C., Levasseur, S., Finno, R.J.. Inverse analysis techniques for parameter identification in simulation of excavation support systems. Computers and Geotechnics 2008;35(3):331–345.

[12] Tang, Y.G., Kung, G.T.C.. Application of nonlinear optimization technique to back analyses of deep excavation. Computers and Geotechnics 2009;36(1-2):276–290. URL http://dx.doi.org/10.1016/j.compgeo.2008.02.004.

[13] Juang, C.H., Luo, Z., Atamturktur, S., Huang, H.. Bayesian updating of soil parameters for braced excavations using field observations. Journal of Geotechnical and Geoenvironmental Engineering 2012;139(3):395–406.

[14] Whittle, A.J., Hashash, Y.M.A., Whitman, R.V.. Analysis of deep excavation in Boston. Journal of geotechnical engineering 1993;119(1):69–90.

[15] Ledesma, A., Gens, A., Alonso, E.E.. Estimation of parameters in geotechnical backanalysis - I. Maximum likelihood approach. Computers and Geotechnics 1996;18(1):1–27. doi:10.1016/0266-352X(95)00021-2. URL http://dx.doi.org/10.1016/0266-352X(95)00021-2.

[16] Gens, A., Ledesma, A., Alonso, E.E.. Estimation of parameters in geotechnical backanalysis - II. Application to a tunnel excavation problem. Computers and Geotechnics 1996;18(1):29–46. doi:10.1016/0266-352X(95)00022-3. URL http://dx.doi.org/10.1016/0266-352X(95)00022-3.

[17] Tarantola, A.. Inverse Problem Theory and Methods for Model Parameter Estimation. Philadelphia: SIAM; 2005.

[18] Kitanidis, P.K.. Bayesian and geostatistical approaches to inverse problems. In: Biegler, L., Biros, G., Ghattas, O., Heinkenschloss, M., Keyes, D., Mallick, B., et al., editors. Large-scale inverse problems and quantification of uncertainty. Chichester, UK: John Wiley & Sons. ISBN 0470685859; 2011, p. 71–85.

[19] Frangos, M., Marzouk, Y.M., Willcox, K., van Bloemen Waanders, B.. Surrogate and reduced-order modeling: A comparison of approaches for large-scale statistical inverse problems. In: Biegler, L., Biros, G., Ghattas, O., Heinkenschloss, M., Keyes, D., Mallick, B., et al., editors. Large-scale inverse problems and quantification of uncertainty. Chichester, UK: John Wiley & Sons; 2011, p. 123–149.

[20] Xiu, D.. Numerical methods for stochastic computations: A spectral method approach. Princeton: Princeton University Press; 2010.

[21] Marzouk, Y.M., Xiu, D.. A stochastic collocation approach to Bayesian inference in inverse problems. Communications in Computational Physics 2009;6(4):826–847. doi:10.4208/cicp.2009.v6.p826. URL http://www.scopus.com/inward/record.url?eid=2-s2.0-74349093769&partnerID=40&md5=2e079a7e16f5d0278

[22] Ghanem, R.G., Spanos, P.D.. Stochastic finite elements: a spectral approach. New York: Springer; 1991.

[23] Le Maître, O.P., Knio, O.M.. Spectral Methods for Uncertainty Quantification with Applications to Computational Fluid Dynamics. New York: Springer; 2010.

[24] Young, G.A., Smith, R.L.. Essentials of statistical inference. 16; Cambridge: Cambridge University Press; 2005. ISBN 0521839718.

[25] Stefanou, G.. The stochastic finite element method: Past, present and future. Computer Methods in Applied Mechanics and Engineering 2009;198(9-12):1031–1051. URL http://www.sciencedirect.com/science/article/pii/S0045782508004118.

[26] Wiener, N.. The Homogeneous Chaos. American Journal of Mathematics 1938;60(4):897–936.

[27] Isukapalli, S.S.. Uncertainty analysis of transport-transportation models. Ph.D. thesis; New Brunswick; 1999.

[28] Sudret, B., Berveiller, M.. Stochastic finite element methods in geotechnical engineering. In: Phoon, K.K., editor. Reliability-based design in geotechnical engineering: computations and applications. New York: Taylor & Francis; 2008, p. 260–297.

[29] Sudret, B.. Global sensitivity analysis using polynomial chaos expansions. Reliability Engineering & System Safety 2008;93(7):964–979.

[30] El Moselhy, T.A., Marzouk, Y.M.. Bayesian inference with optimal maps. Journal of Computational Physics 2012;231(23):7815–7850. doi:http://dx.doi.org/10.1016/j.jcp.2012.07.022. URL http://www.sciencedirect.com/science/article/pii/S0021999112003956.

[31] Boyd, S.P., Vandenberghe, L.. Convex optimization. Cambridge: Cambridge University Press; 2004. ISBN 0521833787.

[32] Niederreiter, H.. Quasi Monte Carlo Methods. Wiley Online Library; 1992. ISBN 047006160X.

[33] von Wolffersdorff, P.A.. Results of field test and evaluation of the predictions and subsequent calculations. 1994.

[34] Mestat, P., Arafati, N.. Modélisation par éléments finis du comportement du rideau de palplanches expérimental de Hochstetten. Bulletin des Laboratoires des Ponts et Chaussé 1998;216:19–39.

[35] Levasseur, S., Malécot, Y., Boulon, M., Flavigny, E.. Soil parameter identification using a genetic algorithm. International Journal for Numerical and Analytical Methods in Geomechanics 2008;32(2):189–213.

[36] Cañavate Grimal, A.. Metodología para la identificación de parámetros en excavaciones profundas al abrigo de muros pantalla mediante métodos espectrales estocásticos. Phd thesis; Universitat Politècnica de València; 2014.

[37] Look, B.G.. Handbook of geotechnical investigation and design tables. London: Taylor & Francis; 2007.

[38] Naval Facilities Engineering Command (NavFac), . Design Manual 7.02. Foundations & Earth Structures. 1986.

[39] Bakker, K.J., Beem, R.C.A.. Modelling of the sheet pile wall test in Karlsruhe 1993. In: Smith, I.M., editor. Proceedings of Third European Conference on Numerical Methods in Geotechnical Engineering - ECONMIG 94. Manchester: Taylor & Francis; 1994,.

[40] Dunnicliff, J.. Geotechnical Instrumentation for Monitoring Field Performance. John Wiley & Sons; 1994. ISBN 9780471005469.

[41] Gens, A.. General report: Prediction, performance and design. In: Shibuya, S., Mitachi, T., Miura, S., editors. Symposium on Pre-Failure Deformation Characteristics of Geomaterials. Rotterdam: Balkema; 1995, p. 1233–1247.